6820–6836 *Nucleic Acids Research, 2022, Vol. 50, No. 12* *Published online 23 June 2022*
https://doi.org/10.1093/nar/gkac469

TEB/*POLQ* plays dual roles in protecting *Arabidopsis* from NO-induced DNA damage

Qiang Lv[1,†], Shuang Han[1,†], Lei Wang[1,2,†], Jinchan Xia[1], Peng Li[1], Ruoyang Hu[1], Jinzheng Wang[1], Lei Gao[1], Yuli Chen[1], Yu Wang[1], Jing Du[1], Fang Bao[1], Yong Hu[1], Xingzhi Xu[1,3], Wei Xiao[1,4,*] and Yikun He[1,*]

[1]College of Life Sciences, Capital Normal University, Beijing 100048, China, [2]Department of Biological Sciences, Mississippi State University, Mississippi State, MS 39762, USA, [3]Guangdong Key Laboratory for Genome Stability & Disease Prevention and Carson International Cancer Center, Shenzhen University School of Medicine, Shenzhen, Guangdong 518060, China and [4]Department of Biochemistry, Microbiology and Immunology, University of Saskatchewan, Saskatoon, SK S7N 5E5, Canada

Received August 29, 2021; Revised May 07, 2022; Editorial Decision May 16, 2022; Accepted June 10, 2022

ABSTRACT

Nitric oxide (NO) is a key player in numerous physiological processes. Excessive NO induces DNA damage, but how plants respond to this damage remains unclear. We screened and identified an *Arabidopsis* NO hypersensitive mutant and found it to be allelic to *TEBICHI*/*POLQ*, encoding DNA polymerase θ. The *teb* mutant plants were preferentially sensitive to NO- and its derivative peroxynitrite-induced DNA damage and subsequent double-strand breaks (DSBs). Inactivation of *TEB* caused the accumulation of spontaneous DSBs largely attributed to endogenous NO and was synergistic to DSB repair pathway mutations with respect to growth. These effects were manifested in the presence of NO-inducing agents and relieved by NO scavengers. NO induced G2/M cell cycle arrest in the *teb* mutant, indicative of stalled replication forks. Genetic analyses indicate that Polθ is required for translesion DNA synthesis across NO-induced lesions, but not oxidation-induced lesions. Whole-genome sequencing revealed that Polθ bypasses NO-induced base adducts in an error-free manner and generates mutations characteristic of Polθ-mediated end joining. Our experimental data collectively suggests that Polθ plays dual roles in protecting plants from NO-induced DNA damage. Since Polθ is conserved in higher eukaryotes, mammalian Polθ may also be required for balancing NO physiological signaling and genotoxicity.

INTRODUCTION

Nitric oxide is an important signalling molecule involved in many physiological processes in mammals and its effects in biological processes depend on its source, duration and concentration. At low doses, NO exerts cytoprotective effects and triggers carcinogenesis, while at high doses, NO has been shown to produce cytotoxic effects and induce apoptosis (1). Similar effects are observed in plants: at low doses, NO promotes development, while at high doses, it suppresses growth (2–4).

NO and its metabolic derivatives like N_2O_3, NO_2 and $ONOO^-$ (peroxynitrite) mainly cause damage to bases (5). For example, N_2O_3 deaminates guanine to xanthine (6), and $ONOO^-$ is a strong oxidant that reacts directly with guanine to produce 8-NO_2-deoxyguanine (8-NO_2-dG), which is unstable and can be depurinated to abasic (AP) sites (7,8). NO-induced damage to bases can be rescued by base-excision repair, which requires the recognition of the adduct by a specialized DNA glycosylase, followed by a strand break at the AP site and local DNA synthesis (9). If unrepaired, NO-induced adducts may block replication and trigger replication fork collapse, leading to double-strand breaks (DSBs). As one of the most dangerous lesions in living cells, DSB is mainly repaired by non-homologous end-joining (NHEJ) during interphase and by homologous recombination (HR) during S and G2 phases when homologous chromatids are available.

Stalled replication forks may trigger cell cycle checkpoints that slow down S phase progression, arrest cells at G2 and enhance the DNA-damage response (DDR) capacity, for example, by inducing relevant gene expression. During this period, the DNA-damage tolerance (DDT) mechanism, which does not remove but rather facilitates bypass

*To whom correspondence should be addressed. Tel: +86 10 68903089; Fax: +86 10 68903089; Email: yhe@cnu.edu.cn
Correspondence may also be addressed to Wei Xiao. Tel: +86 10 68903412; Fax: +86 10 68903412; Email: wei.xiao@usask.ca
†The authors wish it to be known that, in their opinion, the first three authors should be regarded as Joint First Authors.

of the block, is operational at the arrested fork. DDT can be error-free, which utilizes newly synthesized sister chromatids for template switching to bypass the lesion. Alternatively, translesion DNA synthesis (TLS) utilizes specialized TLS polymerases to bypass DNA adducts and avoid replication fork collapse. Because the fidelity of TLS polymerases is lower than that of replicative DNA polymerases, the TLS process often leads to increased mutation (10). In yeast, a lack of Polζ or Rev1 decreases the probability of UV-induced mutations at cyclobutane pyrimidine dimers (CTD) (11,12), while a lack of Polη increases the frequency of UV-induced mutation (13,14). Similarly, *Arabidopsis* Polη, as with its human counterpart, can bypass CTD *in vitro* (15). When *Arabidopsis* plants are irradiated with UV, the somatic mutation rates in *Atrev3*, *Atrev7* (defective in AtPolζ) and *Atrev1* mutants are lower than those in the wild-type, while the mutation rate is higher in *Atpolh* (defective in AtPolη) plants than wild-type plants (16), indicating that there are at least two TLS polymerases in *Arabidopsis* that respond to UV damage with different biological consequences.

POLQ (Polθ) is an A-family DNA polymerase containing an N-terminal helicase-like domain, an unknown central domain and a C-terminal polymerase domain (17). Polθ appears to be able to extend the 3′-OH termini of single- and double-stranded DNA and across AP sites or mismatches in a template-independent manner (18–22). Polθ bypasses various adducts (23) in an error-free (24–26) or error-prone (27–29) manner. Recently, the Polθ polymerase domain was found to possess DNA-end-trimming activity that is required for microhomology-mediated end-joining (30).

Polθ plays an important role in plants. Deletion of *POLQ* in *Chlamydomonas unicellularis* sensitizes the algae to zeocin (31), suggesting that Polθ is involved in DSB repair. Similarly, expression of the moss *POLQ* gene is induced by bleomycin, and *POLQ* deletion mutants are hypersensitive to bleomycin (32). Deletion of *Arabidopsis TEBICHI* (*TEB*)/*POLQ* leads to reduced root growth, hypersensitivity to DNA-damaging agents, delayed G2/M cell cycle progression and constitutively activated DDR (33). Subsequently, *teb* was found to be synergistic with mutations involved in replication checkpoints and HR (34). In addition, *POLQ* deletion in *Arabidopsis* interferes with the insertion of foreign DNA fragments, such as T-DNA, into the genome (35,36). Polθ also participates in the DSB repair induced by CRISPR-Cas9 (37). These observations collectively indicate that, like its mammalian counterpart, the plant Polθ plays an important role in processing DSBs produced from various sources. However, whether and how the plant Polθ is involved in processing base damage and replication blocks remains unclear.

In the process of characterizing *Arabidopsis* NO hypersensitive mutants, we found that one of the corresponding genes is allelic to *TEB*/*POLQ*. Through forward genetic analyses, it was demonstrated that *Arabidopsis* Polθ indeed protects against spontaneous and NO-induced DSB damage. Furthermore, Polθ appears to be required for TLS across lesions caused by NO derivatives like $ONOO^-$. As Polθ is highly conserved, the roles Polθ plays in protecting against NO toxicity may be common to higher eukaryotes, including plants and animals.

MATERIALS AND METHODS

Plant materials and generation of mutant plants

All the mutants in this study were in the *Arabidopsis thaliana* ecotype Columbia-0 (Col-0) background. The NO-sensitive mutant *sno2-1*/*teb-6* were isolated from an EMS-induced mutant pool and backcrossed for three times as described previously (38). Another allelic mutant *sno2-2*/*teb-7* were isolated as described (39). The T-DNA-inserted alleles *teb-2* (SALK_035610), *teb-3* (SALK_001669), *teb-4* (SALK_037552), *teb-5* (SALK_018851), *teb-8* (SALK_200962), *rad51d* (CS830262), *lig4* (SALK_044027), *ku70* (SALK_123114), *xrcc2* (SALK_029106), *rev3* (SALK_029237) and *polh* (SALK_129731) were obtained from the Arabidopsis Biological Resource Center (https://abrc.osu.edu) as previously described (33,34,40,41). Lines carrying homozygous T-DNA insertion mutations were established, and the presence of T-DNA was confirmed by genomic DNA PCR using the primer sets listed in Supplementary Table S1. The *gsnor1-3*, *cue1-5* and *noa1* mutants have been described (42,43). For genetic analyses, the double and triple mutants were generated by standard genetic crosses and were identified in F2 progeny by genomic PCR and phenotypic observation.

In all experiments, plant seeds were surface sterilized with 10% bleach for 10 min and washed five times at least with sterile water before sowing. Plants were grown on plates containing 1/2× Murashige and Skoog (MS) medium, 1% (w/v) sucrose, 0.7% (w/v) agar, 0.05% (w/v) 2-(*N*-morpholino) ethanesulfonic acid (MES, pH 5.7). After a 3-day incubation at 4°C in dark, the plates were placed vertically in the growth chamber (100 μmol m^{-2} s^{-1}; 16-h-light/8-h-dark cycle; 22°C) until analysis.

For different chemical treatments, the plants were grown in the 1/2× MS medium supplemented with sodium nitroprusside (SNP, Sigma-Aldrich), old SNP (44), potassium ferricyanide (Sigma), *S*-nitroso-*N*-acetylpenicillamine (SNAP, Sigma), 2-phenel-4,4,5,5-tetramethy-limidazoline-1-oxyl-3-oxide (c-PTIO, Sigma-Aldrich and Abcam), zeocin (Invitrogen), Hemoglobin (Beyotime), hydrogen peroxide (H_2O_2), methyl viologen (MV, Sigma), NaCl, mannitol, $CdCl_2$ or N_ω-nitro-L-arginine (L-NNA, Sigma-Aldrich) under indicated conditions for 10–14 days, and the lengths of primary roots were determined using ImageJ (http://rsb.info.nih.gov/ij/).

To test the sensitivity of plants to $ONOO^-$-related agents, 5-day-old seedlings preincubated on 1/2× MS plates were transferred to liquid 1/2× MS medium containing various concentrations of SNP, 3-morpholinosydnonimine-*N*-ethylcarbamide (SIN-1, Cayman), ebselen (Cayman) or c-PTIO, incubated for an additional 2–4 days and then the lengths of the primary roots and chlorophyll content were measured.

NO and $ONOO^-$ measurement

NO levels were measured in roots using the fluorescent NO indicator dye 3-amino, 4-aminomethyl-2′,7′-difluorofluorescein diacetate (DAF-FM DA, Sigma-Aldrich) as described previously (45). Briefly, seedling

roots were incubated in 10 mM Tris–HCl (pH 7.4) for 30 min, followed by staining with 10 μM DAF-FM DA for 30 min in the dark. After washing three times with 10 mM Tris–HCl for 5 min each, the roots were mounted on a microscope slide and analyzed under a microscope (Nikon ECLIPSE NI) equipped with a charge-coupled device camera (excitation, 495 nm; acquisition, 515 nm). $ONOO^-$ levels were detected in roots using a similar method except for using the $ONOO^-$-specific fluorescent dye 2-[6-(4-aminophenoxy)-3-oxo-3*H*-xanthen-9-yl]-benzoic acid (APF, Cayman). The signal intensity was quantified using ImageJ.

SNO2 gene mapping

The NO-sensitive mutants (M3 generation; Col-0 background) were crossed with Landsberg *erecta* wild-type plants. DNA was extracted from 1,034 NO-sensitive mutant plants selected from the F2 plant population based on their NO-hypersensitive phenotype upon treatment with 50 μM SNP, and analyzed using simple sequence length polymorphism and cleavage-amplified polymorphic sequence markers (46).

Root morphology analysis

To observe root tip structures, roots of 6-day-old seedlings grown in medium with or without SNP were stained with 10 μg/ml PI for 1 min, washed with water twice and images were captured using a confocal fluorescence microscope (LSM510; Zeiss) with excitation and emission wavelengths of 559 and 619 nm, respectively. At least 10 plants per line were observed.

Promoter GUS activity analyses

To study the *TEB* promoter with a GUS activity assay, a 0.7-kb *TEB* promoter sequence was amplified from Col-0 genomic DNA using primers *TEB* promoter-F and *TEB* promoter-R (Supplementary Table S2). The amplified DNA fragments were purified with a gel extraction kit (Omega) and subcloned into the pBlunt plasmid (Transgene) in accordance with the manufacturer's protocol. The cloned genomic DNA fragment was confirmed by sequencing and then subcloned into the destination vector pCambia1301, which harbours the *GUS* reporter gene. The resulting plasmid was mobilized into *Agrobacterium tumefaciens* (GV3101) and used to transform Col-0 plants using the floral dip method. Transformants were selected on 1/2× MS salt plates containing 1% sucrose and 25 μg/ml hygromycin. T3 transformants harbouring homozygous T-DNA inserts were used for the GUS activity assay.

To detect GUS activity, seedlings were stained with a solution containing 100 mM Na_2HPO_4, pH 7.0, 0.1% Triton X-100, 2 mM $K_3Fe[CN]_6$, 2 mM $K_4Fe[CN]_6$, and 0.5 mg/ml 5-bromo-4-chloro-3-indolyl-β-D-glucuronic acid (X-gluc) for 1 h at 37°C in the dark. The GUS-stained seedlings were treated with 70% and then 96% ethanol followed by embedding in a clearing solution (80% chloral hydrate and 10% glycerol) and analysis by microscopy (Axio Zoom.V16, Zeiss).

Subcellular localization assay

For a transient expression assay, the *TEB*-coding region was amplified using primers *TEB* CDS-F and *TEB* CDS-R (Supplementary Table S2) and cloned into plasmid pCambia1300-GFP as a GFP fusion. Then the construct was delivered into the *Arabidopsis* protoplasts via a method as described previously (47). The GFP fluorescence was observed under a confocal fluorescence microscope (LSM510, Zeiss).

Chlorophyll content determination

After various chemical treatments, seedlings were weighed and placed in appropriate amount of 90% (v/v) acetone for extraction. The chlorophyll content was determined by measuring the absorbance at 652, 665 and 750 nm using a spectrophotometer.

Gene expression analysis

Total RNA was extracted from various tissues as indicated by a TRIZOL reagent (Invitrogen). 1 μg of the total RNA was used for cDNA synthesis using a PrimeScript Reagent Kit with gDNA eraser (TaKaRa). Quantitative RT-PCR (qRT-PCR) for *TEB*, DSB-inducible and cell cycle-related genes was performed using SYBR Premix Ex*Taq* II (TaKaRa) on an Applied Biosystems 7500 Fast real-time PCR system (Applied Biosystems). The gene-specific primer sets were listed in Supplementary Table S3 and the housekeeping gene *SAND* (44) and *ACTIN8* were used as internal controls. The program was at 95 °C for 10 min, 40 cycles of 95°C for 15 s and 60°C for 1 min, followed by 95°C for 15 s and 60°C for 15 s. Three technical replicates were performed with each sample and the expression level was calculated by the $2^{-\Delta\Delta Ct}$ method (48).

Apurinic/apyrimidinic (AP or abasic) site analysis

Total genomic DNA was extracted from 7-day-old seedlings preincubated on vertical MS plates with or without another day of SNP, MV or SIN-1 treatment using the DNeasy Plant Mini Kit (Qiagen). The AP number was quantified with an OxiSelect Oxidative DNA Damage Quantitation Kit (AP sites, BioCells, STA-324) following manufacturer's instructions.

In vitro single-strand DNA break assay

A previously published protocol (49) was followed to quantify single-strand breaks in close-circular plasmid pET28a DNA.

Cell ploidy analysis

The nuclei were extracted from the seedlings and analysed by flow cytometry as previously described (50).

Histone preparation and γ-H2AX immunoassay

Histones were extracted from nuclear preparations of seedlings as previously described (51). Protein samples

were subjected to SDS-PAGE, blotted, and immunodetected with a rabbit monoclonal anti-γ-H2AX antibody at 1:2500 dilution (Abcam, ab81299) and rabbit polyclonal anti-Histone H3 antibodies (Abcam, ab1791) at 1:2500 dilution. Slide preparation, immunostaining and quantification of γ-H2AX foci were performed as previously described (52). Briefly, root tips were fixed for 45 min in 4% paraformaldehyde in PME (50 mM PIPES, pH 6.9, 5 mM $MgSO_4$, and 1 mM EGTA) and then washed 3 × 5 min in PME. Tips were digested for 30 min in a 1% (w/v) cellulase solution in PME and then washed 3 times in PME. These roots were gently squashed onto slides, air dried, and stored at -80°C. Each slide was incubated overnight at 4°C with 100 μl anti-γ-H2AX antiserum. Slides were washed 3 times in PBS solution and then incubated for 2 h at room temperature in 100 μl blocking buffer consisting of Alexa 488-conjugated goat anti-rabbit secondary antibodies. Finally, slides were washed 3 times in PBS and mounted in Vectashield mounting medium with 4′,6-diamidino-2-phenylindole (DAPI).

Comet assay

Comet assays were performed as described (50,53). Briefly, the seedlings were chopped into pieces with a razor blade in 500 μl 1 × PBS buffer supplemented with 20 mM EDTA on ice. The nucleus suspension was filtered into a new tube through a 50 μm nylon mesh, combined with low-melting agarose at a ratio of 1:1, and pipetted onto CometSlides. After incubation in lysis solution for 1 h at 4°C, the slides were placed in 1× Tris-acetate electrophoresis buffer for 30 min prior to electrophoresis in the same buffer for 10 min at 4°C. The nuclei were stained with SYBR Green I. Images were captured and quantified with CometScore software (Tritek Co.), and at least 50 nuclei were scored per slide.

DNA extraction and whole-genome sequencing (WGS)

The genomic DNA from 14-d-old Col-0, *teb-6*, *teb-5* and *rev3* seedlings on medium with or without 15 nM MV or 25 μM SNP was extracted based on the CTAB protocol (54). The tissues were grounded to powder in liquid nitrogen, transferred to a preheated (65°C) CTAB lysis buffer and mixed by vortex. The samples were centrifuged at 10,000 rpm at room temperature (RT) for 5 min after incubating at 65°C for 60 min. The supernatant was extracted with equal volume of phenol/chloroform/isopentanol (25:24:1) followed by centrifuging at 10,000 rpm at RT for 10 min. Approximately 70% volume of precooled (-20°C) isopropanol was added and put at -20°C for more than 2 h to precipitate the DNA, followed by centrifuging at 12,000 rpm for 15 min at RT. 75% ethanol was added to wash the pellet and removed by centrifugation, and the DNA pellet was air-dried for 3–5 min. The pellet was dissolved by 30–200 μl TE buffer for further study. After DNA extraction, 1 μg genomic DNA was randomly fragmented by Covaris, followed by fragments selection by Agencourt AMPure XP-Medium kit to an average size of 200–400 bp. Selected fragments were end repaired and 3′ adenylated, and the adaptors were ligated to the ends of these 3′ adenylated fragments. The products were amplified by PCR and purified by the Agencourt AMPure XP-Medium kit. The purified double-strand PCR products were heat denatured to single strand, and then circularized by the splint oligo sequence. The single-strand circle DNA (ssCir DNA) was formatted as the final library and qualified by QC. The final qualified libraries were sequenced by BGISEQ-500. ssCir DNA molecule formed a DNA nanoball (DNB) containing >300 copies through rolling-cycle replication. The DNBs were loaded into the patterned nanoarray by using high density DNA nanochip technology. Finally, pair-end 100 bp reads were obtained by combinatorial Probe-Anchor Synthesis (cPAS).

Variant calling

The GATK best practices pipeline was used to analyze the 12 *Arabidopsis* samples. Briefly, the raw read files were quality checked and trimmed with Trimmomatic (v0.39). The trimmed reads were mapped to the *A. thaliana* TAIR10 reference genome with Burrows-Wheeler Aligner (v0.7.17-r1188). The format conversions and removal of duplicated reads were done with Samtools (v1.10) and Picard (v22.4) (http://broadinstitute.github.io/picard/), respectively. Variants were detected separately with GATK (v 4.1.7.0) and later merged with the function CombineVariants. A known *Arabidopsis* variation dataset from the 1001 genomes project (55) was introduced to annotate our SNVs at this step. A customized script was implemented to identify transition or transversion.

Statistical analysis

Statistical analyses were performed using software GraphPad Prism version 6.01 and SPSS23. P-value, sample number, and adjusted P-value are included in figures or figure legends.

RESULTS

SNO2 mutant is specifically sensitive to NO

To elucidate molecular mechanisms of NO signal response in plants, we used SNP, a well-established NO donor, to screen an existing *Arabidopsis* mutant library (38) and obtained a genetically stable NO-sensitive mutant designated *sensitive to nitric oxide 2* (*sno2-1*). Under normal culture conditions, the root length of the *sno2-1* mutant was approximately 70% that of the wild-type (Figure 1A), and *sno2-1* plants were hypersensitive to SNP (Figure 1A–C). As the *sno2-1* mutant did not display increased sensitivity to chemicals like potassium ferricyanide [$K_3Fe(CN)_6$] or old SNP (containing no NO but nitrate, nitrite and ferrocyanide) (44), the inhibitory effect was unlikely due to other components (such as cyanide) being released from SNP (Figure 1D) (56). The application of SNAP, another NO donor, and c-PTIO, a specific scavenger of NO, further confirmed that NO was responsible for the NO sensitive phenotype of *sno2-1* (Figure 1E). Compared with wild-type plants, *sno2-1* was no more sensitive to H_2O_2 or MV (Supplementary Figure S1A and B), indicating that the NO-sensitive phenotype of *sno2-1* is unrelated to reactive oxygen species (ROS). The *sno2-1* mutants also did not display

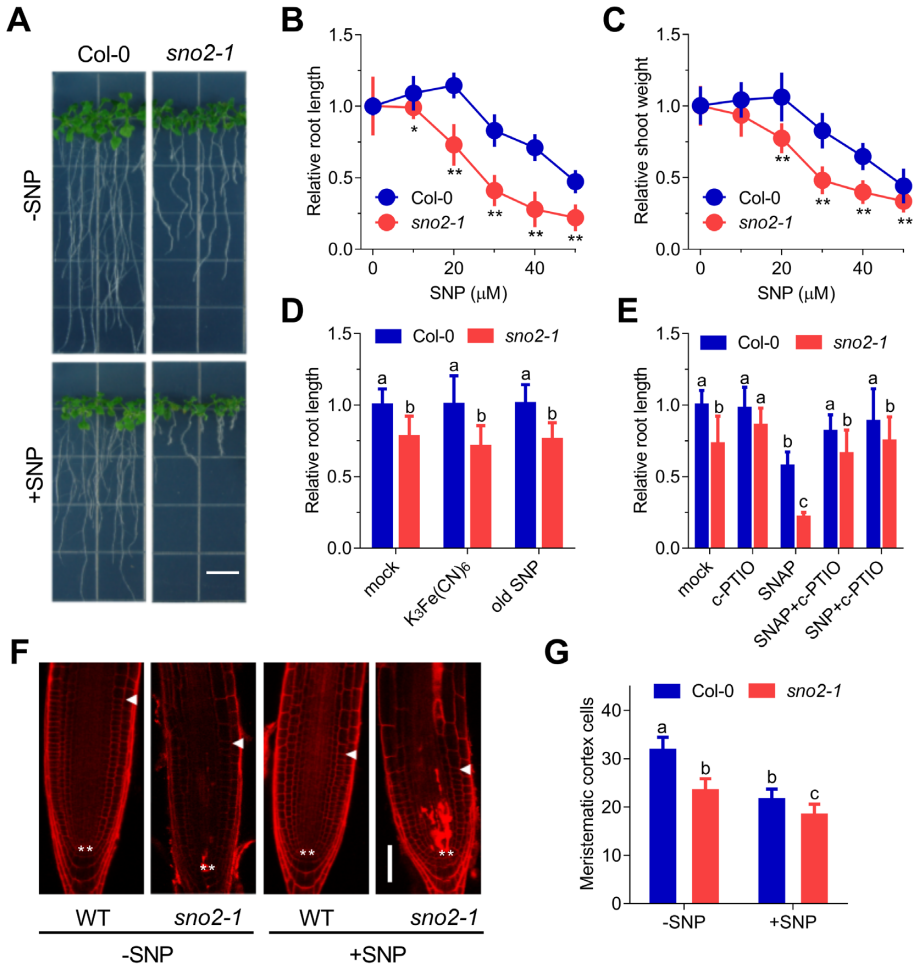

Figure 1. Phenotypes of Arabidopsis *sno2-1* mutants under NO treatment. (**A**) Col-0 (WT, wild-type) and *sno2-1* seedlings grown in medium with or without 40 μM of the NO donor sodium nitroprusside (SNP) for 14 d. Scale bars = 1 cm. (**B** and **C**) Dose-dependent effects of SNP on the growth of roots (B) and shoots (C) of Col-0 and *sno2-1* seedlings. The relative primary root length and shoot weight of 14-d-old seedlings grown in medium containing various concentrations of SNP. Values are ratios relative to the value under 0 μM SNP conditions (n = 13–19, means ± SD, $^*P < 0.05$, $^{**}P < 0.01$, compared with the corresponding Col-0, two-tailed Student's t-test). (**D**) Col-0 and *sno2-1* seedlings grown in medium containing 50 μM $K_3Fe(CN)_6$ or 50 μM old SNP for 10 days (n = 15, means ± SD, $P < 0.05$, one-way ANOVA and Tukey's HSD). (**E**) Col-0 and *sno2-1* seedlings grown in medium containing 200 μM c-PTIO, 50 μM SNP, 50 μM SNAP and combinations of these for 10 days (n = 13, means ± SD, $P < 0.05$, one-way ANOVA and Tukey's HSD). (**F**) Representative confocal images showing root tips of Col-0 and *sno2-1* seedlings grown in medium with or without 50 μM SNP for 6 d. PI staining was used to visualize cell walls and completely stained cells are dead. Triangles indicate the cortex meristem size from quiescent center (indicated by asterisks) to elongating cells. Scale bars = 50 μm. (**G**) Effects of SNP on cortex cells in the root meristematic zone. Col-0 and *sno2-1* seedlings were grown as in (F). Cortex cells in the meristematic zone were counted under a confocal microscope. Data shown are means ± SD (n = 11, $P < 0.05$, one-way ANOVA and Tukey's HSD).

increased sensitivity to NaCl, osmotic stress or cadmium (Supplementary Figure S1C), demonstrating that *sno2-1* is specifically sensitive to NO. Unlike wild-type plants, approximately 67% (12/18) of the *sno2-1* mutants contained dead cells in the meristem zone of the root tips, as judged by propidium iodide (PI) staining. This phenomenon was aggravated by SNP treatment (Figure 1F), when the meristem zone of *sno2-1* decreased significantly (Figure 1G), indicating that *SNO2* protected root tips from exogenous NO-induced cell-cycle arrest and/or cell death in the meristem zone.

SNO2 alleviates endogenous NO-induced growth inhibition

To assess whether *sno2-1* is also hypersensitive to the accumulation of endogenous NO, *sno2-1* was crossed with *cue1-5* (3) and *gsnor1-3* (43) mutants known to have elevated endogenous NO levels to obtain the corresponding double mutants. There were no significant differences in the NO content between *sno2-1* and the wild-type plants; however, the NO content in *sno2-1 cue1* was significantly higher than that of wild-type plants but similar to that of *cue1* (Figure 2A–D), indicating that the inactivation of *SNO2* did not alter endogenous NO levels. However, the growth of the aerial parts and roots of *sno2-1 cue1* was significantly inhibited in comparison to that of the *cue1* single mutant (Figure 2A and B). c-PTIO and L-NNA (a NOS inhibitor) effectively rescued the phenotype of *sno2-1 cue1* (Figure 2E), demonstrating that the retarted growth of *sno2-1cue1* was due to intolerance to the endogenous NO. The inhibitory effect was even more exacerbated in *sno2-1 gsnor1* plants than in *sno2-1 cue1*, as the normal development of the true leaf

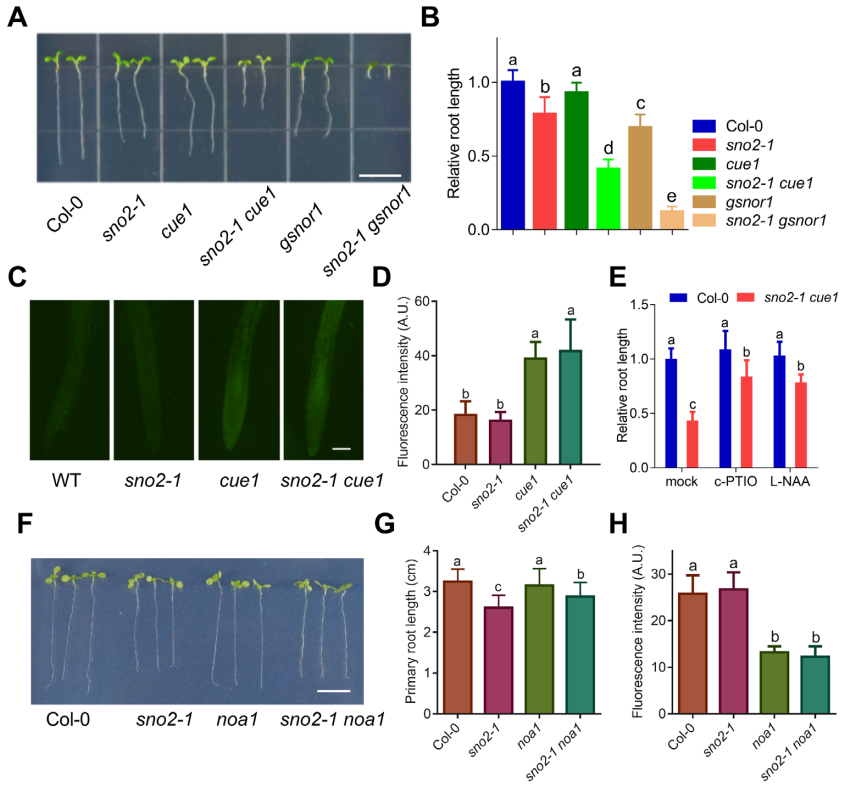

Figure 2. *SNO2* alleviates growth inhibition by endogenous NO. (**A**) Col-0, *sno2-1*, *cue1*, *sno2-1 cue1*, *gsnor1* and *sno2-1 gsnor1* seedlings grown for 7 days. Scale bars = 1 cm. (**B**) Relative primary root lengths of Col-0, *sno2-1*, *cue1*, *sno2-1 cue1*, *gsnor1* and *sno2-1 gsnor1* seedlings as shown in (A). Data shown are means ± SD (n = 16–22) relative to Col-0 plants. Letters represent significant differences ($P < 0.05$, one-way ANOVA and Tukey's HSD). (**C**) NO contents in Col-0, *sno2-1*, *cue1* and *sno2-1 cue1* root tips as measured by DAF-FM DA. Scale bars = 100 μm. (**D**) Quantitative analysis of results shown in (C) expressed as arbitrary units (A.U.) using ImageJ software (n = 15, means ± SD; $P < 0.05$, one-way ANOVA and Tukey's HSD). (**E**) Relative root lengths of wild-type (Col-0) and *sno2-1 cue1* plants grown in medium supplemented with 200 μM c-PTIO and 100 μM L-NNA for 10 days (n = 15, $P < 0.05$, one-way ANOVA and Tukey's HSD). (**F**) Col-0, *sno2-1*, *noa1* and *sno2-1 noa1* seedlings grown in normal medium for 10 days. Scale bars = 1 cm. (**G**) The primary root length of Col-0, *sno2-1*, *noa1* and *sno2-1 noa1* seedlings as shown in (F). Data shown are expressed as means ± SD (n = 16–22). Different letters represent significant differences ($P < 0.05$, one-way ANOVA and Tukey's HSD). (**H**) NO content in Col-0, *sno2-1*, *noa1* and *sno2-1 noa1* seedlings root tips as measured by DAF-FM DA. Results shown are in arbitrary units (A.U.) using ImageJ software (n = 12, means ± SD; $P < 0.05$, one-way ANOVA and Tukey's HSD).

and elongation of the primary root were severely impaired, leading to rapid death of *sno2-1 gsnor1* plants (Figure 2A and B). Inactivation of NOA1, a GTPase involved in NOS-like pathway (57), could partially restore the *sno2-1* mutant phenotype (Figure 2F–H), indicating that the growth defect in *sno2-1* was due to accumulated NO. Together with the effect of c-PTIO treatment (Figure 1E), our observations collectively imply that *SNO2* effectively protects plants from endogenous NO toxicity.

sno2 is allelic to *TEB*/*POLQ*

Using a map-based cloning strategy, we located the *sno2-1* mutation to the *TEB* gene encoding Polθ (33), with a C2971T single-nucleotide substitution on exon 13 resulting in a nonsense mutation (Supplementary Figure S2A and B). The *sno2-1* mutation in *TEB* was further confirmed by *Bse*MII digestion, which cleaved the wild-type sequence but not that of *sno2-1* (Supplementary Figure S2B and C). *sno2-2* contains a G3204A mutation on exon 14 at the *TEB* locus (Supplementary Figure S2D), causing a nonsense mutation and increased NO sensitivity comparable to *sno2-1* (Supplementary Figure S3). Five available *TEB* T-DNA insertion lines, SALK_035610, SALK_001669, SALK_037552, SALK_018851 and SALK_200962, designated *teb-2*, *teb-3*, *teb-4*, *teb-5* and *teb-8*, respectively, were confirmed by genomic DNA PCR (Supplementary Figure S2E) and further characterized by qRT-PCR using five pairs of primers (Supplementary Figure S2A and F). *teb-5* abolished transcription at all five locations; *teb-2* and *teb-8* transcripts could only be detected by the N-terminal primer pair; all three mutants displayed increased NO sensitivity reminiscent of *sno2-1* and *sno2-2* (Supplementary Figure S3). Hence, the above five lines are considered null mutants, and we designated *sno2-1* and *sno2-2* as *teb-6* and *teb-7*, respectively from herein. As anticipated, *teb-4* contains a T-DNA insertion at the very C-terminus and its transcript was detected by all five pairs of primers. To our surprise, the *teb-3* transcript was also detected by all primer pairs (Supplementary Figure S2F), which was further confirmed by two '*trans*-T-DNA insertion' primer pairs F5 + R5 and F6 + R6 (Supplementary Figure S2G). Consistently, *teb-3* displayed no obvious growth defect and very moderate sensitivity to SNP treatment (Supplementary Figure S3).

Based on the assumption that *teb-3* contains a T-DNA insertion at the C-terminal polymerase domain, it was previously concluded that the polymerase activity of Polθ is dispensable for normal plant growth (33). To ask whether the N-terminal helicase domain alone is sufficient to support plant growth, we grew plant seedlings in the presence of novobiocin (NVB) that selectively binds to and inhibits the Polθ ATPase activity (58), and found that NVB treatment of *teb-3* plants phenocopies *teb* null mutants under both untreated and SNP-treated conditions (Supplementary Figure S4). Hence, the Polθ helicase activity appears to be essential to protect plants from endogenous and exogenous NO toxicity.

To further explore the relationship between NO and *TEB*, the expression of *TEB* in response to SNP treatment was monitored. A dose-response study (Supplementary Figure S5A) found that *TEB* expression was induced by SNP in a dose-dependent manner, while a time-course study (Supplementary Figure S5B) revealed that *TEB* expression was induced by 100 μM SNP during a period of 6–24 h, after which its mRNA level plateaued up to 48 h. A high-level *TEB* expression was observed in the shoot apical meristem, vascular tissue of roots and leaves, trichomes, anthers and stigma in Pro_{TEB}*:GUS* transgenic plants (Supplementary Figure S6A), and its relative expression in different tissues as measured by qRT-PCR showed the similar pattern (Supplementary Figure S6B). Transient expression of Pro_{35S}*:TEB-GFP* in *Arabidopsis* protoplasts showed that TEB-GFP was located in the nucleus (Supplementary Figure S6C), consistent with its known activities (59,60).

Teb/*sno2* is hypersensitive to NO-induced DSBs

Arabidopsis TEB is homologous to *Drosophila MUS308* and mammalian *POLQ*. Previous studies showed that Polθ is involved in DSB repair in animals and now named Polθ-mediated end joining (TMEJ) (17,61,62). The *Arabidopsis teb* mutant is sensitive to mitomycin C (MMC) and methyl methanesulfonate (MMS) (33). MMC causes inter-strand crosslinks and MMS mainly causes replication blocks, both of which result in DSBs if not repaired in a timely manner. To ask if Polθ is directly involved in DSB repair, we grew plants in the presence of zeocin, which specifically induces strand breaks (63) and found that the *teb-6* mutant root growth was indeed potently inhibited by zeocin in a dose-dependent manner (Figure 3A and B). We tested a hypothesis that NO induces DSBs by performing a neutral comet assay to visualize DSBs. SNP treatment induced comet tails; however, more DSBs were found in the *teb-6* mutants than in wild-type plants (Figure 3C and D). The cellular histone H2AX phosphorylation (γ-H2AX) level serves as a reliable marker of DSB (51). The number of γ-H2AX foci in *teb-6* root tips was much more than wild-type plants after treatment with SNP or zeocin (Supplementary Figure S7). Consistently, immunoblotting data revealed that *teb-6* mutants accumulated much more DSBs than wild-type upon SNP and zeocin treatment (Figure 3E). Furthermore, the γ-H2AX band began to appear after 6-h SNP treatment in wild-type plants, while it was detected after 1-h SNP treatment in the *teb-6* mutant plants, which were inhibited by the NO scavenger c-PTIO (Supplementary Figure S8A). SNP treatment also induced the expression of *BRCA1* (Supplementary Figure S8B) and *GR1* (Supplementary Figure S8C), which were also inhibited by c-PTIO, particularly in the *teb-6* mutant, suggesting that Polθ prevents NO-induced DSBs accumulation in *Arabidopsis*.

To further ascertain if the *teb-6* mutant accumulated spontaneous and NO-induced DSBs, we examined the expression level of a panel of DDR marker genes known to be induced after γ-ray irradiation (64,65). It is apparent from Figure 3F that the *teb-6* mutation induced the expression of all DDR marker genes examined; in addition, the expressions of genes involved in DSB sensing and repair, including *RAD51*, *BRCA1*, *GR1* (mammalian *CtIP* ortholog), *PARP1*, *PARP2* and *ATM*, were further induced by SNP. These results indicate that spontaneous DNA damage was accumulated in *teb-6* mutant plants, and that NO treatment further increased the level of DNA damage, most likely in the form of DSBs. Furthermore, the expression of *GR1* was found to be increased in *cue1* and *gsnor1* mutants (Figure 3G), but *GR1* and *PARP1* were reduced in *noa1* (Figure 3H), indicating that endogenous NO could cause DNA damage. The above data supports a notion that TEB can restrain DNA damage induced by NO.

Deletions at the DSB containing microhomology at the junction are characteristic mutational signature associated with TMEJ repair. In an attempt to understand impacts of plant Polθ on TMEJ, we performed WGS and found more deletions with microhomology in the SNP-induced wild-type genome (17/44) than in *teb-6* (7/39) and *teb-5* (7/32) (Supplementary Figure S9A and B). Templated insertions (TINs) at the break site are characteristic genomic scars associated with TMEJ repair (62,66,67). SNP induced more direct or inverted repeat TINs in wild-type (15/58) than in *teb-6* (3/59) and *teb-5* (2/49) mutants (Supplementary Figure S9C and D).

Genetic interactions between *tebs* and DSB repair pathway mutations

To address roles of Polθ in the protection against DSBs, we examined genetic relationships between *TEB* and major DSB repair genes. DSB is one of the most severe types of DNA damage in animal and plant cells, and NHEJ and HR are considered to be the two major DSB repair pathways (68). The *teb-6* mutation moderately affected plant growth (Figures 1A and 4A). Remarkably, while *ku70* and *lig4* mutations defective in the NHEJ pathway, did not alter normal growth, they strongly enhanced the impaired developmental phenotype of *teb-6* and *teb-5*. The *teb-6 ku70*, *teb-6 lig4*, *teb-5 ku70* and *teb-5 lig4* double mutants exhibited severe growth retardation, much shorter roots than *teb-6*, and more severe morphological defects in the leaves (Figure 4A and B). The roots of *teb-6 lig4* were extremely twisted, and the root tips contained many dead cells (Figure 4C).

The *lig4 xrcc2* double mutation still did not affect normal plant growth (Supplementary Figures S10A–D), but the homozygous *teb-6 lig4 xrcc2* triple mutant appeared to be lethal (Figure 4D). A *teb-6*$^{-/-}$ *lig4*$^{+/-}$ *xrcc2*$^{-/-}$ heterozygote was used to obtain homozygous triple mutants, but they died soon after germination (Figure 4D), indicating that the growth-inhibition effect of *teb-6* mutation is

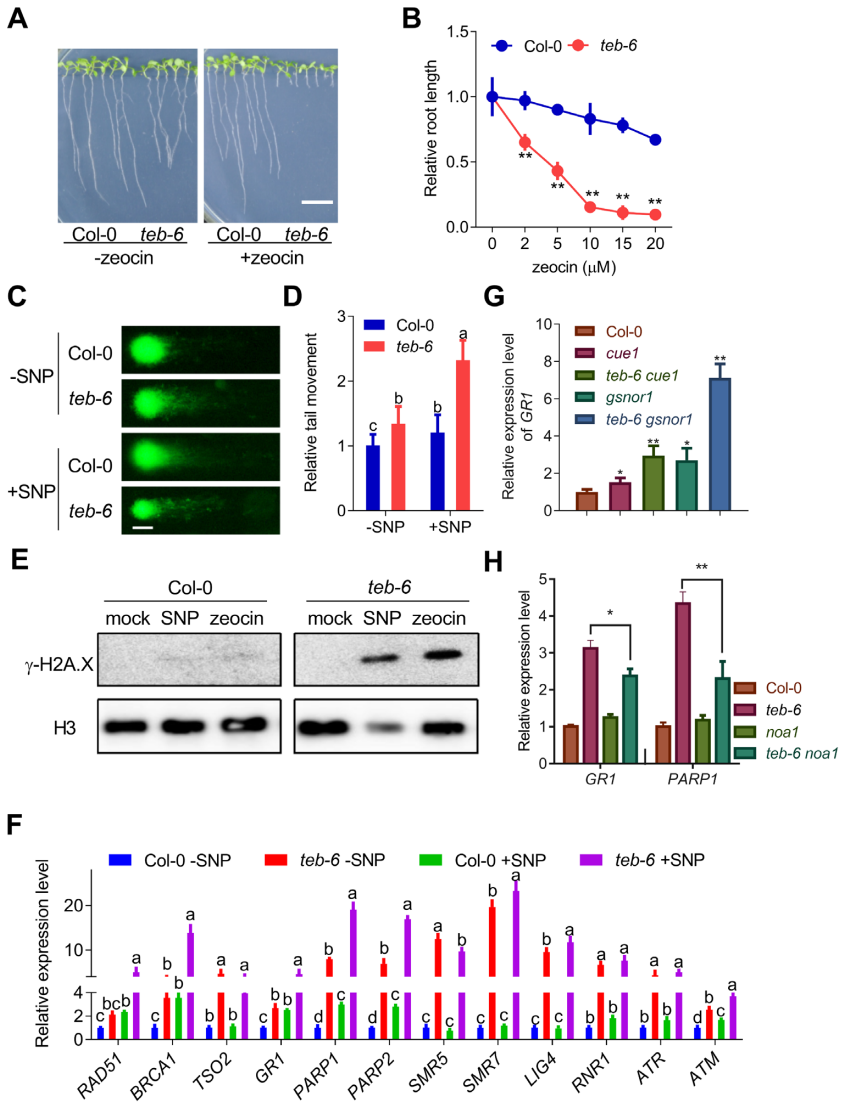

Figure 3. Roles of Polθ in protecting spontaneous and NO-induced DSBs. (**A**) Col-0 and *teb-6* seedlings grown in medium with or without 10 μM zeocin for 10 days. Scale bars = 1 cm. (**B**) Effects of zeocin treatment on root elongation in wild-type Col-0 and *teb-6* seedlings. Root length data are expressed as means ± SD ($n = 15$, $^{**}P < 0.01$, compared with Col-0, two-tailed Student's *t*-test). (**C**) Representative comet assay images for SNP-induced toxicity. The images show the degree of DNA damage inflicted on single nuclei from 5-d-old Col-0 and *teb-6* seedlings treated with 0 μM or 100 μM SNP for 48 h. The intensity of the dispersed signal in the tail indicates severity of DNA damage. Scale bars = 20 μm. (**D**) Quantitative analysis of olive tail moments to reflecting the extent of DSBs in the nucleus. Values are relative to Col-0 plants grown in the absence of SNP. Data are expressed as means ± SD from at least 50 comets. Different letters represent significant differences ($P < 0.05$, one-way ANOVA and Tukey's HSD). (**E**) Accumulation of γ-H2AX in Col-0 and *teb-6* seedlings after treatments with 100 μM SNP and 10 μM zeocin for 24 h. Histone H3 served as a loading control. Two images were from the same gel. Similar results were obtained in at least two separate experiments. (**F**) DNA damage-inducible gene expression in response to SNP. Histogram of relative gene expression levels in wild-type and *teb-6* plants on qRT-PCR analysis. At least 50 plants were used per replicate. Data were normalized to *SAND* mRNA levels in the same samples and are expressed as means ± SD (n = 3) relative to untreated Col-0 seedlings. Different letters represent significant differences ($P < 0.05$, one-way ANOVA and Tukey's HSD). (**G**) Relative *GR1* expression in *cue1*, *teb-6 cue1*, *gsnor1* and *teb-6 gsnor1* ($n = 3$, $^{*}P < 0.05$, $^{**}P < 0.01$, compared with Col-0, two-tailed Student's *t*-test). (**H**) Relative *GR1* and *PARP1* expression in Col-0, *teb-6*, *noa1* and *teb-6 noa1* seedlings ($n = 3$, $^{*}P < 0.05$, $^{**}P < 0.01$, compared with Col-0, two-tailed Student's *t*-test).

jointly exacerbated by *lig4* and *xrcc2* mutations. We then used the weak *teb-6* mutant allele *teb-3* (SALK_001669) to create a homozygous *teb-3 lig4 xrcc2* triple mutant. While *teb-3* did not show noticeable growth defects, the growth of *teb-3 lig4 xrcc2* triple mutant was severely inhibited, albert completed their life cycle (Supplementary Figure S10A–D), indicating that the *teb-3 lig4 xrcc2* plants also accumulated endogenous DSBs. In comparison to the *teb-3* single and *lig4 xrcc2* double mutants, the corresponding triple mutant was much more sensitive to SNP (Supplementary Figure S10C and D).

The growth of major HR pathway mutants such as *xrcc2* and *rad51d* was comparable to wild-type plants; however, root growth in *teb-6 xrcc2, teb-6 rad51d* and *teb-5 xrcc2* plants was strongly inhibited, albeit to a lesser extent than in *teb-6 ku70* and *teb-6 lig4* (Figure 4A and B), which is consistent with a previous report (34). Furthermore, a large area of cell death was observed in the root meristematic

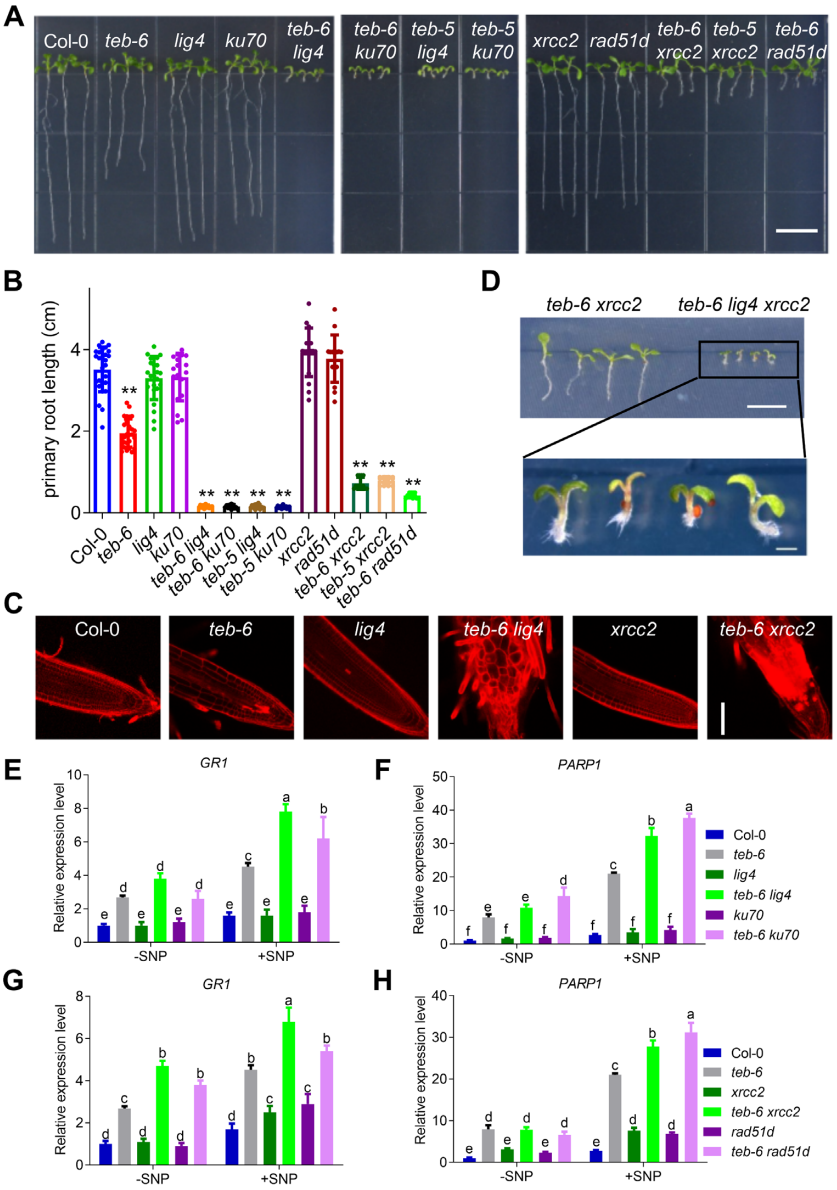

Figure 4. Genetic interactions between *teb-6* and DSB repair pathway mutations. (**A**) Representative images of Col-0 and indicated mutant seedlings grown for 10 d. Scale bars = 1 cm. (**B**) Quantitative analysis of the primary root length of 10-d-old seedlings grown as described in (A) (n = 12–27, means ± SD, $^{**}P < 0.01$, compared with Col-0, two-tailed Student's t-test). (**C**) Representative images of PI staining (red) to visualize the cell walls in root tips of Col-0 and indicated mutant seedlings grown for 10 days. Completely stained cells are dead. Scale bars = 50 μm. (**D**) Representative image of *teb-6 xrcc2* and *teb-6 lig4 xrcc2* seedlings grown for 7 days (upper panel, scale bars = 1 cm) and its enlargement (lower panel, scale bars = 1 mm). (**E**–**H**) Relative expression of *GR1* (E and G) and *PARP1* (F and H) in *teb-6*, *lig4*, *teb-6 lig4*, *ku70* and *teb-6 ku70* seedlings (E and F), and *xrcc2*, *teb-6 xrcc2*, *rad51d* and *teb-6 rad51d* seedlings (G and H) in response to SNP as determined by qRT-PCR analysis. At least 50 plants were used per replicate. Data were normalized to *SAND* mRNA levels in the same samples and expressed as means ± SD (n = 3) relative to untreated Col-0. Different letters represent significant differences ($P < 0.05$, one-way ANOVA and Tukey's HSD).

zone of *teb-6 xrcc2* (Figure 4C). NO scavengers c-PTIO and hemoglobin (Hb) partially alleviated growth defect phenotype of *teb-6 lig4* and *teb-6 xrcc2* double mutants (Supplementary Figure S11A). Therefore, the simultaneous loss of Polθ and c-NHEJ, or Polθ and HR, resulted in an intolerance to NO-induced DSBs, leading to the severe inhibition of plant growth and development.

The expression of *GR1* and *PARP1* was examined in seedlings of various mutants grown with or without SNP treatment. The *teb-6* mutation caused a significant elevation of *GR1* and *PARP1* transcript levels. In sharp contrast, mutations affecting NHEJ (e.g. *lig4*, *ku70*) and HR (e.g. *xrcc2*, *rad51d*) had no effect on the spontaneous *GR1* and *PARP1* expression (Figure 4E–H). Furthermore, NHEJ pathway mutations did not further induce *GR1*, but mildly elevated *PARP1* expression in the *teb-6* background (Figure 4E and F); instead, HR pathway deficiency moderately elevated *GR1* but not *PARP1* expression in *teb-6* mutants (Figure 4G and H). SNP treatment elevated *GR1* and *PARP1* expression in *teb-6* and HR pathway mutants, but not in NHEJ

pathway mutants (Figure 4E–H). In all cases, SNP treatment induced *GR1* and *PARP1* expression in the double mutants in comparison to the corresponding single mutants (Figure 4E–H). As expected, cPTIO and Hb treatments reduced the *BRCA1* and *GR1* expression in *teb-6 lig4* and *teb-6 xrcc2* mutants (Supplementary Figure S11B and C). Similarly, *teb-3* and *lig4 xrcc2* mutations slightly increased the basal-level *PARP1* but not *GR1* expression; the corresponding triple mutation strongly induced *GR1* and *PARP1* expression, which was further exacerbated by treatment with SNP (Supplementary Figure S11D). The above observations collectively indicate that *tebs* and mutations in the DSB repair pathways are synergistic with respect to spontaneous and NO-induced DSB accumulation.

teb-6 is sensitive to NO-derived $ONOO^-$

In animals, NO and O_2^- can be rapidly converted into $ONOO^-$ (69). Within a certain concentration range (e.g. at the μM level), $ONOO^-$ is toxic to animal cells but does not have an obvious toxic effect on plant cells (70), implying the presence of a detoxification mechanism in plants that protects against $ONOO^-$- induced cell death. To ask whether $ONOO^-$ is indeed an important metabolic intermediate after NO treatment, and whether Polθ protects against $ONOO^-$- induced genotoxicity, we first established a detection system in which SIN-1 (a peroxynitrite donor)-induced $ONOO^-$ in root tips could be specifically detected by the fluorescent dye APF (Figure 5A and B). Under the same experimental conditions, SNP also induced a strong APF fluorescent signal that could be eliminated by treatment with an $ONOO^-$ scavenger ebselen (Figure 5A and B), indicating that NO produces $ONOO^-$. Treatment with 5 mM SIN-1 had a devastating effect on the growth of *teb-6* plants (Figure 5C and D), while the root growth of *teb-6* was sensitive to SIN-1 in a dose-dependent manner that was alleviated by ebselen and the NO scavenger c-PTIO (Figure 5E). Because *PARP1* expression was induced by SIN-1 and enhanced further by the inactivation of *TEB* (Figure 5F), and the ebselen treatment partially restored SIN-1 and SNP induced *BRCA1* and *GR1* expression in *teb-6* (Supplementary Figure S12), we concluded that Polθ indeed plays a critical role in protecting plants from DNA damage by NO-derived $ONOO^-$.

SIN-1 directly induced DNA single strand breaks (SSBs) *in vitro*, indicating that $ONOO^-$ is capable of causing DNA strand breaks; however, more strand breaks were observed when Fapy glycosylase (FPG) was used to treat plasmid DNA incubated with SNP or SIN-1 (Figure 5G), indicating that the majority of the DNA damage caused by SNP and SIN-1 was in the form of dG adducts that were recognized and processed by FPG. Furthermore, treatment of wild-type and *teb-6* plants with SNP or SIN-1 induced the formation of AP sites that were comparable to those seen with oxidative damage, indicative of DNA base damage by NO and its derivative $ONOO^-$ that lead to increased depurination (Figure 5H).

NO induces G2/M cell cycle arrest

A variety of genotoxicities activate checkpoint systems to arrest the progression of the cell cycle (50,71). We speculated that DNA damage caused by both endogenous and environmental NO could activate this checkpoint. Checkpoint activation was first assessed by the expression of G2/M phase marker genes, including *CYCB1;1*, *CYCA1;1*, *CYCA2;1*, *CYCA2;2*, *CYCA2;3*, *CYCA2;4*, *CDKA1* and *CDKB2;1*. Compared to wild-type plants, the expression of all marker genes was elevated in *teb-6* (Figure 6A). SNP treatment alone did not induce the above marker gene but significantly increased their expression in the *teb-6* plants, indicating that G2/M arrest can be induced by NO and that Polθ is required to avoid such arrest. Consistently, NO stalled *teb-6* mutant root cells at the G2/M phase, as revealed by a *CYCB1;1-GUS* transgenic reporter (Figure 6B). G2/M phase arrest often induces early cell maturation and promotes endoreduplication (50,72). A flow cytometry assay showed that the proportion of 8C and 16C cells was moderately increased in *teb-6* mutants and was further elevated by SNP treatment (Figure 6C). Hence, Polθ appears to function at the G2 phase to prevent NO-induced DNA damage.

Error-free TLS by Polθ protects against NO-induced DNA damage

Our observations that the *teb* and NO jointly trigger the G2/M phase checkpoint and cell cycle arrest suggest that NO toxicity causes replication fork arrest. As purified mammalian Polθ has TLS activity (26–28,73), and TLS primarily functions at the G2 phase (74,75) through DDT, in which the replication block is bypassed but the adduct is not removed (76), we hypothesized that Polθ plays a critical role in bypassing the NO-induced lesion. To test this hypothesis, we measured the relative sensitivity of *teb-6* and two other TLS polymerase mutants *polh* and *rev3* to SNP. Because NO-derivatives such as $ONOO^-$ can cause DNA oxidative damage (49,77), we also performed parallel MV treatment for comparison. As previously observed, the *teb-6* single mutant grew more slowly than the wild-type plants, while *rev3* and *polh* single mutations or even the *rev3 polh* double mutation did not affect plant growth (Figure 7A). However, the *teb-6 rev3* double and *teb-6 rev3 polh* triple mutants showed more severe growth defects than their respective single and double mutants (Figure 7A), implying that Polθ plays a major role in tolerating spontaneous DNA damage, while Polη and Polζ play backup roles. After SNP treatment, both *teb-6* and *rev3* mutants showed increased sensitivity, and the two mutations were additive (Figure 7A and B), indicating that Polθ and Polζ bypassed the NO-induced DNA adduct(s) via different pathways. Interestingly, *rev3 polh*, *teb-6 polh* and *teb-6 rev3 polh* mutants were no more sensitive to SNP than their corresponding single and double mutants (Figure 7A and B), indicating that Polη is not involved in TLS of NO-induced DNA damage. In sharp contrast, *teb-6*, either alone or in combination with other TLS mutations, did not increase sensitivity to the MV treatment (Figure 7A and B), suggesting that Polθ is not primarily responsible for TLS of oxidative DNA damage.

Knowing that Polθ plays a critical role in bypassing NO-induced lesions, we attempted to understand its effects on mutagenesis and the mutational spectrum by whole-genome sequencing (WGS) using TAIR10 as a reference genome. Treatment of wild-type plants with SNP induced

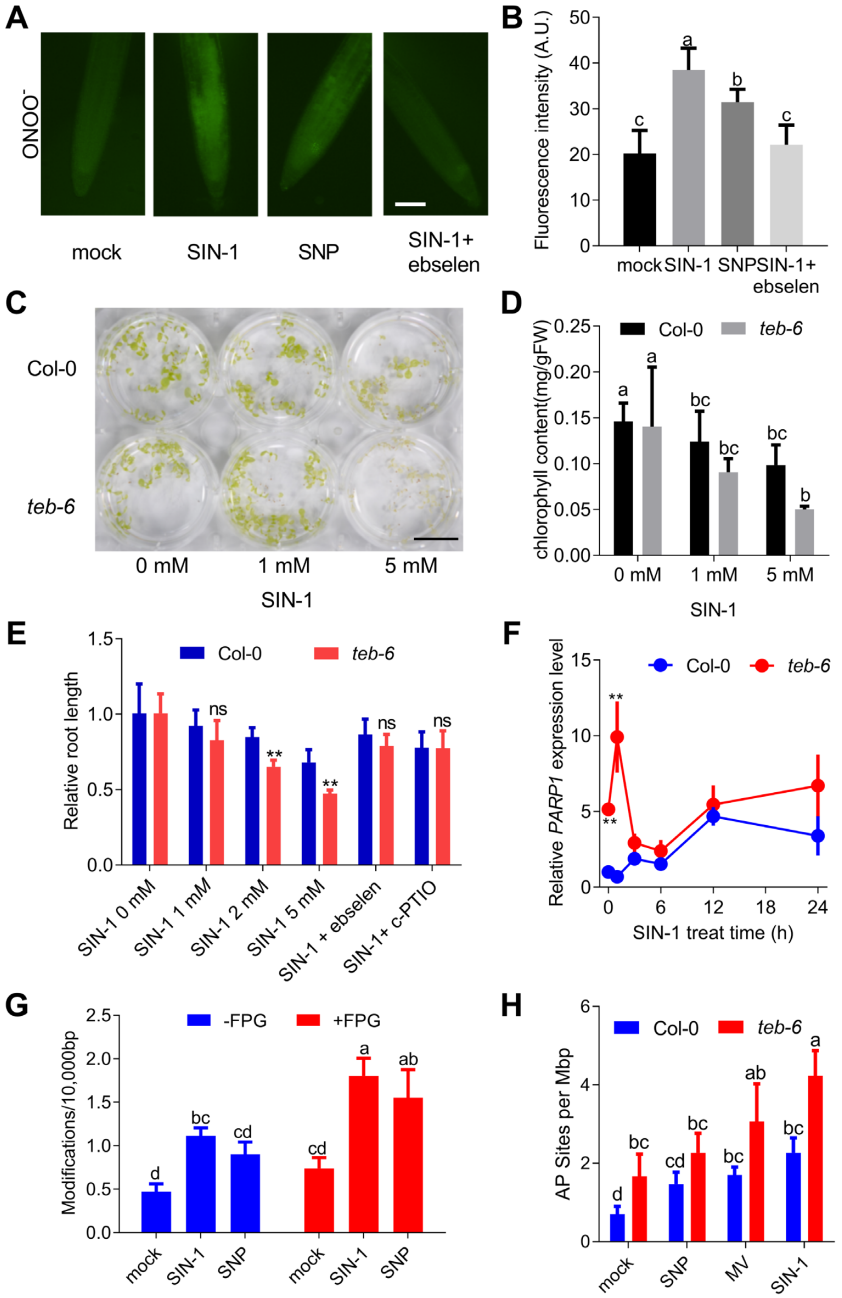

Figure 5. Phenotypes of Arabidopsis *teb-6* mutants under SIN-1 treatment. (**A**) Representative images showing fluorescence intensity of peroxynitrite in root tips of 7-day-old *Arabidopsis* seedlings exposed to 1 mM SIN-1, 50 μM SNP and 50 μM SNP + 20 μM ebselen in liquid medium for 12 h. Scale bars = 50 μm. (**B**) Quantitative analysis of results shown in (A) expressed as arbitrary units (A.U.) using ImageJ software (n = 23–24, means ± SD; $P < 0.05$, one-way ANOVA and Tukey's HSD). (**C**) Phenotypes of 7-day-old wild-type (Col-0) and *teb-6* plants were transplanted to the liquid medium supplemented with or without SIN-1 for another 5 d. Scale bars = 1 cm. (**D**) Quantitative analysis of chlorophyll contents in wild-type (Col-0) and *teb-6* as shown in (C) (n = 3, means ± SD; $P < 0.05$, one-way ANOVA and Tukey's HSD). FW, fresh weight. (**E**) Relative root length of wild-type (Col-0) and *teb-6* plants grown in liquid medium supplemented with 1, 2 and 5 mM SIN-1, 500 μM c-PTIO and 20 μM ebselen as described as in (C) (n = 12, average ± SD; $^{**}P < 0.01$, compared with Col-0, Student's t-test; ns no significant difference). (**F**) Relative *PARP1* expression in 10-day-old wild-type (Col-0) and *teb-6* seedlings grown in liquid medium supplemented with 3 mM SIN-1 for different time periods (n = 3, $^{**}P < 0.01$, untreated Col-0 served as a control, two-tailed Student's t-test). (**G**) DNA damage of pET28a plasmid was induced by 50 μM SNP or 10 μM SIN-1 in phosphate buffer (pH 7.4) with or without 8 units *E. coli* Fapy glycosylase (FPG) for 1 h (n = 3, average ± SD; $P < 0.05$, one-way ANOVA and Tukey's HSD). (**H**) AP sites in 5-d-old wild-type and *teb-6* seedlings grown in liquid medium supplemented with 50 μM SNP, 30 nM MV or 2 mM SIN-1 for another 2 days. Results are expressed as mean number of AP sites per Mbp genomic DNA ± SD (n = 3; $P < 0.05$, one-way ANOVA and Tukey's HSD).

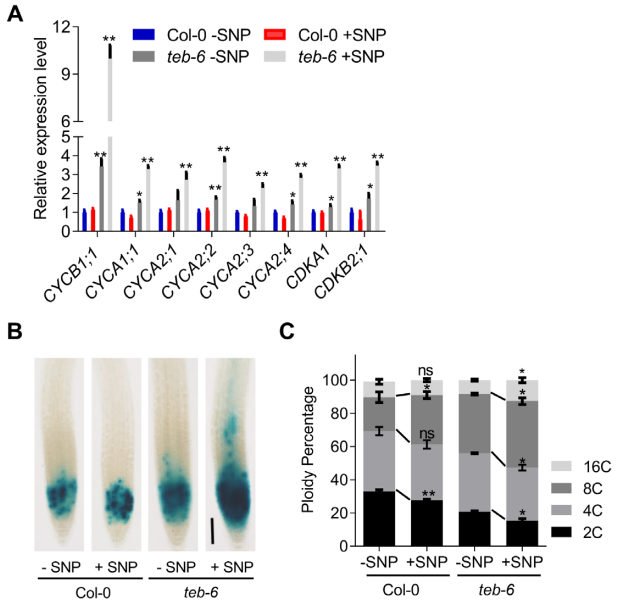

Figure 6. Effects of SNP on mitotic activities of *teb-6* mutants. (**A**) 7-d-old wild-type and *teb-6* seedlings untreated (mock) or treated with 100 μM SNP for 48 h. Expression of cell-cycle-related genes as determined by qRT-PCR. Data shown are normalized to levels of *SAND* mRNA in the same samples (n = 3, means ± SD, $*P < 0.05$, $**P < 0.01$, untreated Col-0 served as a control, two-tailed Student's *t*-test). (**B**) Representative images of GUS-stained root tips of wild-type (Col-0) and *teb-6 CYCB1;1:GUS* transgenic plants grown as described in (A). Scale bars = 100 mm. (**C**) Effects of SNP on cell ploidy in Col-0 and *teb-6* seedlings grown as described in (A). Data shown are means ± SD for ∼8000 nuclei per group ($n = 3$, $*P < 0.05$, $**P < 0.01$, ns, no significance, untreated Col-0 and *teb-6* served as a control, two-tailed Student's *t*-test).

19.11×10^{-5} single-nucleotide substitutions per read, which were raised by 16% in *teb-6* and 15% in *teb-5*, but not significantly increased in *rev3* (Figure 7C and Supplementary Table S4). This observation is consistent with a hypothesis that Polθ is involved in error-free TLS across NO-induced lesions. In contrast, the single nucleotide variants (SNVs) induced by MV were increased by 12%, 14% and 17% in the *teb-6*, *teb-5* and *rev3* mutants, comparing with 9% increase in Col-0 with no statistically significant difference (Figure 7C and Supplementary Table S4).

NO treatment of DNA *in vitro* and in cultured human cells mainly causes G:C > T:A, A:T > G:C and G:C > A:T mutations (78). Indeed, these were major types of substitutions induced by both SNP and MV in wild-type plants (Supplementary Table S4). The *teb-6* and *teb-5* mutations proportionally increased SNP-induced G:C > T:A, G:C > A:T and A:T > T:A substitutions but had little effect on other types of base substitutions (Figure 7D). In comparison, the *rev3* mutation did not appear to have a clear mutational signature in response to SNP- and MV-induced DNA damage, other than an increase in G:C > T:A and G:C > A:T mutations (Figure 7D and E), consistent with previous reports that guanine is the major base targeted by SNP (79). The above mutagenesis analyses collectively supported our general conclusion that plant Polθ specifically acts on NO-induced DNA damage in a largely error-free manner.

DISCUSSION

Our previous studies showed that excessive NO inhibits *Arabidopsis* root growth, most likely by reducing the number of meristem cells (3,80), but the underlying mechanisms were obscure. Through the isolation and characterization of an NO hypersensitive mutant *teb-6*, the current study has led us to conclude that excessive NO inhibits plant growth by primarily inducing DNA damage. Firstly, the comet assay and γ-H2AX assays revealed that NO induces DNA DSBs. Secondly, the expression of a panel of known DNA-damage responsive genes was induced upon the treatment of plants with NO. Thirdly, NO induced cell death in the stem cell niche around the quiescent root centre, which is characteristic of DNA damage (81). Fourthly, NO treatment arrested cell-cycle progression at the G2/M phase and induced cycle-related gene expression in the *teb-6* mutant. Fifthly, expression of the *TEB* was induced by NO at the transcriptional level. Finally, *TEB* was found to encode DNA Polθ, whose known functions to date are exclusively involved in DNA metabolism (17,82).

Since both *teb-6* and *teb-7* produced wild-type level full-length transcripts and their premature translation termination occurs between the N-terminal helicase domain and C-terminal polymerase domain, yet they displayed null mutant phenotypes, we infer that the polymerase activity of plant Polθ is absolutely required to protect NO-induced DNA damage. On the other hand, *teb-1*, a helicase-defective but polymerase-intact mutant, also displayed growth defects (33). Together with our observation that the chemical inhibition of the Polθ ATPase activity displayed the *teb* null mutant phenotype, we cautiously conclude that both polymerase and helicase activities of Polθ are required for the protection against NO-induced DNA damage, although this conclusion is subject to further examination.

Our observations that spontaneous and NO-induced DSBs accumulated in the *teb-6* mutant indicate that Polθ protects *Arabidopsis* from this type of DNA damage. However, it remains unclear whether Polθ prevents DSB formation or if it is required for the repair of DSBs, or both. As a matter of fact, Polθ has been reported to function both ways in mammalian cells. Polθ is a TLS polymerase required for bypassing various DNA adducts (24–28,73), many of which are replication-blocking lesions. Failure to bypass such lesions at the stalked replication fork causes fork collapse, resulting in DSBs. However, Polθ can also extend single-strand and double-strand termini or process damaged termini, priming them for DSB repair. Loss of any of the above activities would be synergistic with defects in NHEJ and HR with respect to plant growth and viability, concurring with the striking phenotype observed in this study. Results obtained from this study provide evidence that Polθ plays a critical role in protecting plant cells from NO-induced endogenous DNA damage, since *teb* plant displayed moderate growth retardation, while mutants in c-NHEJ, HR and other TLS pathways did not. When facing excessive endogenous (e.g. in *cue1* or *gsnor1* mutants) and/or exogenous NO-induced DNA adducts, Polθ is required to prevent the formation of DSBs. Polθ, as a TLS polymerase, can use damaged DNA, including DNA adducts, AP sites or even strand termini, as a template to prime replication.

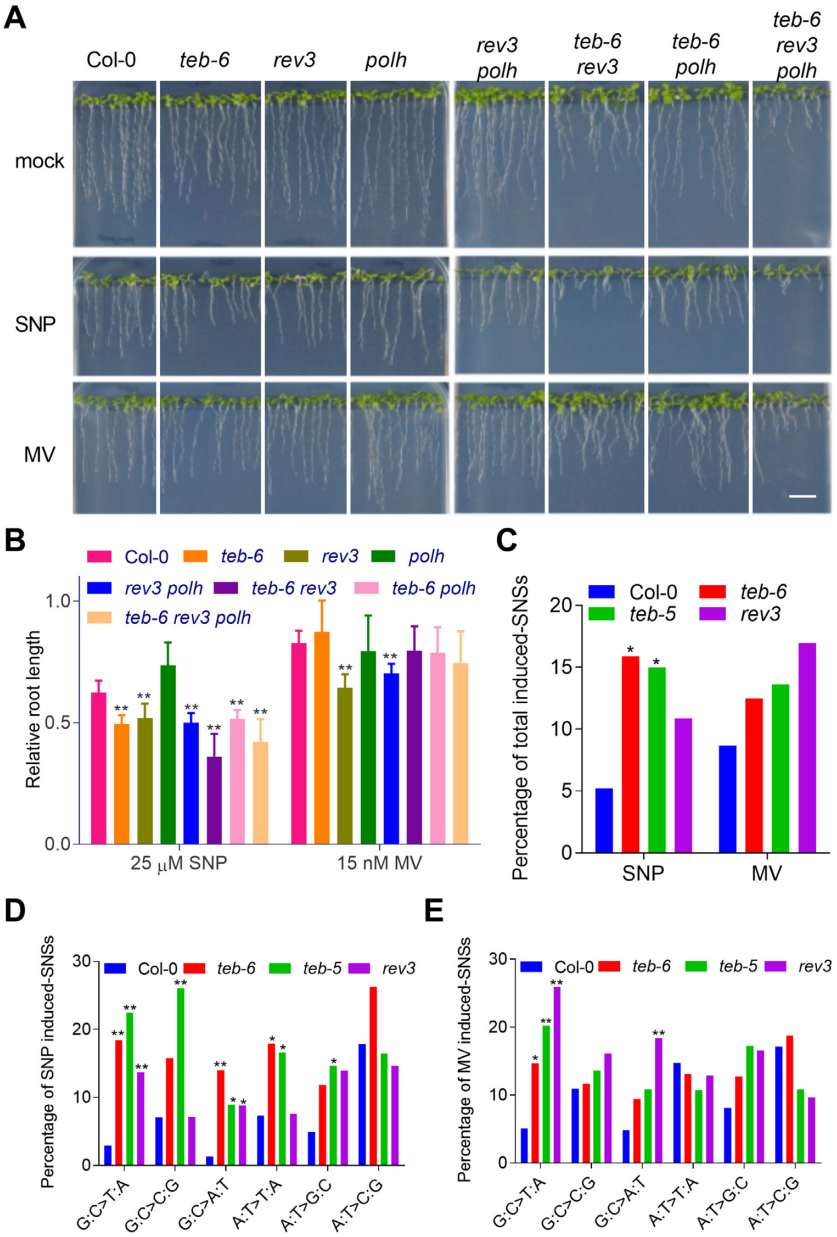

Figure 7. Involvement of Polθ in response to SNP-induced lesions. (**A**) Representative images showing root growth of 10-d-old wild-type (Col-0) and indicated mutants grown on medium with or without 25 μM SNP or 15 nM MV. Scale bars = 1 cm. (**B**) Quantitative analysis of root length of plants shown in (**A**) relative to untreated wild-type plants. Data represent mean ± SD ($n = 12$; $^{**}P < 0.01$, compared with Col-0, two-tailed Student's *t*-test). (**C**) SNP- and MV-induced single-nucleotide substitutions in wild-type, *teb-6*, *teb-5* and *rev3* plants. P values were calculated using the Fisher's exact test, * $P < 0.05$. The genomic DNA from 14-day-old Col-0, *teb-6*, *teb-5* and *rev3* seedlings on medium with or without 25 μM SNP or 15 nM MV was extracted. (**D** and **E**) Distribution of SNP- and MV-induced single-nucleotide substitutions in wild-type, *teb-6*, *teb-5* and *rev3* plants. P values were calculated using the Fisher's exact test, * $P < 0.05$, ** $P < 0.01$.

This study demonstrated that Polθ is preferentially involved in the TLS of NO-induced lesions, while in the absence of Polθ, other TLS polymerases, such as Polζ, could serve backup roles. Our observation of plant *rev3* sensitivity to NO is consistent with a report that chicken DT40 cells deficient in Rev3 are hypersensitive to NO (83). Our conclusion on the involvement of *Arabidopsis* Polθ in TLS relief of replication stress agrees with a very recent report (84). Although this study revealed that Polθ is required to prevent oxidation-induced signature G:C > T:A transversions, we could not rule out the possibility that it is also required for TLS bypassing other types of DNA damage like its mammalian counterparts (24–28,73). It has been reported that mammalian Polθ possesses a 5′dRP lyase activity within its C-terminal polymerase domain (85), and chicken DT40 cells lacking Polθ and Polβ are sensitive to MMS due to reduced base excision repair (BER) activity (86). Our observations cannot rule out the possibility that Polθ protects plants from NO-induced DNA damage through BER, particularly since the *Arabidopsis* genome lacks an ortholog en-

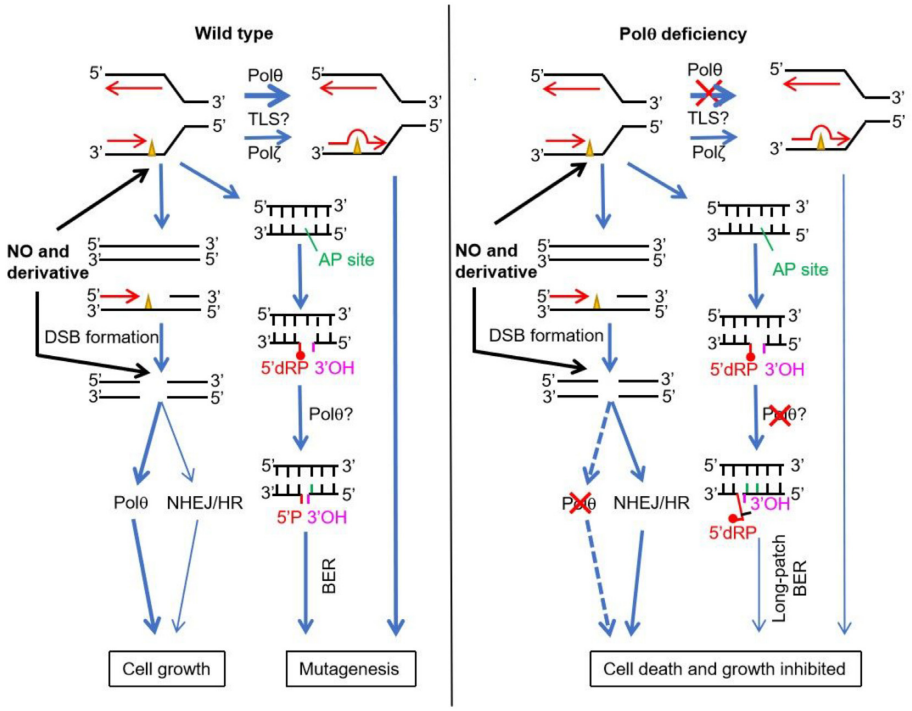

Figure 8. A working model of AtPolθ-mediated responses to NO-induced DNA damage. Polθ plays multiple roles in dealing with NO-induced DNA lesions. Firstly, Polθ and Polζ jointly bypass NO-induced and stalled replication blocks through largely error-free TLS; lack of such activities may result in replication fork collapse and DSBs. Secondly, Polθ may have a 5'dRP lyase activity and participate in base excision repair (BER). Thirdly, Polθ is directly involved in processing spontaneous and NO-induced DSBs; lack of such an activity causes plants to rely heavily on HR and NHEJ for growth or even survival. Hence, Polθ plays a crucial role in maintaining genomic stability, particularly in response to NO-induced lesions. Thin and dash lines represent reduced and lost activities, respectively.

coding Polβ (87), making Polθ an attractive candidate for the source of dRPase activity.

It remains unclear how excessive NO induces DNA damage in plants. In mammals, NO and its derivatives, e.g. N_2O_3 and $ONOO^-$, induce DNA adducts, AP sites and strand breaks (77). *In vitro,* NO-derived $ONOO^-$ induces the formation of 8-oxo-dG and 8-NO_2-dG; the former is rapidly depurinated (88). This study revealed that, although *in vitro* treatment of plasmid DNA with the $ONOO^-$ donor SIN-1 induced nicks, the vast majority of nicks were generated by combined treatment with FPG and SNP or SIN-1, indicating that the adduct(s) are recognized and processed by FPG to produce single-strand breaks, reminiscent of the previously reported induction of DNA oxidative adducts by $ONOO^-$ (89,90). The *Arabidopsis* genome contains FPG and OGG1 orthologs (91) capable of processing the above $ONOO^-$-induced adducts. This study also revealed that SNP and SIN-1 induced AP sites *in vivo* in *Arabidopsis*, suggesting that, similar to in mammals, NO-mediated DNA damage and toxicity in plants depend at least partly on the NO metabolite $ONOO^-$.

NO and reactive nitrogen species (RNS) produces more complex base modifications than ROS and leads to a variety of base substitutions. Although NO gas and NO donor-induced mutational spectra differ, as judged from the *supF* reporter assays in bacterial and human cells, G:C > T:A, A:T > G:C and G:C > A:T are always the most frequent mutations (92). While such an assay is currently unavailable for use in plants, we took a next-generation sequencing approach and found that NO mainly induced G:C > T:A, A:T > G:C, A:T > T:A and G:C > A:T base substitutions in wild-type plants. In addition, our WGS data revealed both reduced TMEJ signature mutations and increased G:C > T:A and G:C > A:T mutations in *teb* lines, further supporting dual roles of plant Polθ in DSB repair and TLS in response to NO-induced lesions. It is interesting to note that mutations accumulate in *A. thaliana* lineages grown at elevated temperatures and in high-salinity soil (93), two environmental stresses known to cause NO and ROS accumulation (94,95), implying that NO contributes to such processes. Indeed, *teb* mutants displayed certain degrees of salt sensitivity (84), reminiscent of their increased NO sensitivity as revealed in this study, suggesting that Polθ also plays a critical role in the protection against high-salinity stress.

In conclusion, we propose a working model (Figure 8) for the involvement of Polθ and other DDR pathways in response to NO toxicity. Under normal growth conditions, endogenous NO-induced toxicity is mainly processed by Polθ, lack of which results in moderate growth retardation, while mutations in other relevant pathways do not. When excessive NO is accumulated either due to NO metabolic mutations (e.g. *cue1* or *gsnor1*) or by treatment with NO-inducing agents, Polθ becomes pivotal for plant growth and survival, while other pathways may also contribute to the detoxification. The dual defects of Polθ and other TLS polymerases, particularly Polζ, result in increased sensitivity to endogenous NO stress, which can be further exacerbated

by exogenous sources of NO. Inactivation of Polθ results in DSB accumulation, either due to NO-induced replication fork collapse or an inability to process strand termini, which requires NHEJ during G1/S phase and HR during G2/M phase to maintain *teb* plant viability. Although not experimentally addressed in this study, plant Polθ may also possess a 5'dRP lyase activity like mammalian Polθ, which can be used to process NO-induced base damage through BER for detoxification. As NO is also an important signalling molecule in other organisms, particularly mammals, the findings in this study may shed light on ways to investigate the novel roles of Polθ in other organisms.

DATA AVAILABILITY

The raw sequence data reported in this paper have been deposited in the Genome Sequence Archive (96) in National Genomics Data Center (97), China National Center for Bioinformation / Beijing Institute of Genomics, Chinese Academy of Sciences, under accession number CRA004785 that are publicly accessible at https://ngdc.cncb.ac.cn/gsa. Shared URL: https://ngdc.cncb.ac.cn/gsa/s/5e1Y111k.

SUPPLEMENTARY DATA

Supplementary Data are available at NAR Online.

ACKNOWLEDGEMENTS

We would like to thank the Arabidopsis Biological Resource Center for the T-DNA inserted mutants. We thank Dr Hailong Wang and Xiangxi He from Capital Normal University for supplying technical support. We also thank Dr Min Zhang from Capital Normal University, for supplying pCambia1300-GFP vector.

FUNDING

National Natural Science Foundation of China [31530006, 31970658]. Funding for open access charge: National Natural Science Foundation of China [31530006, 31970658].
Conflict of interest statement. None declared.

REFERENCES

1. Choudhari,S.K., Chaudhary,M., Bagde,S., Gadbail,A.R. and Joshi,V. (2013) Nitric oxide and cancer: a review. *World J. Surg. Oncol.*, **11**, 118.
2. Beligni,M. and Lamattina,L. (1999) Is nitric oxide toxic or protective? *Trends Plant Sci.*, **4**, 299–300.
3. He,Y., Tang,R.H., Hao,Y., Stevens,R.D., Cook,C.W., Ahn,S.M., Jing,L., Yang,Z., Chen,L., Guo,F. *et al.* (2004) Nitric oxide represses the Arabidopsis floral transition. *Science*, **305**, 1968–1971.
4. Liu,W.Z., Kong,D.D., Gu,X.X., Gao,H.B., Wang,J.Z., Xia,M., Gao,Q., Tian,L.L., Xu,Z.H., Bao,F. *et al.* (2013) Cytokinins can act as suppressors of nitric oxide in Arabidopsis. *Proc. Natl. Acad. Sci. U.S.A.*, **110**, 1548–1553.
5. Thomas,S., Lowe,J.E., Knowles,R.G., Green,I.C. and Green,M.H. (1998) Factors affecting the DNA damaging activity of superoxide and nitric oxide. *Mutat. Res.*, **402**, 77–84.
6. Nguyen,T., Brunson,D., Crespi,C.L., Penman,B.W., Wishnok,J.S. and Tannenbaum,S.R. (1992) DNA damage and mutation in human cells exposed to nitric oxide in vitro. *Proc. Natl. Acad. Sci. U.S.A.*, **89**, 3030–3034.
7. Yermilov,V., Rubio,J. and Ohshima,H. (1995) Formation of 8-nitroguanine in DNA treated with peroxynitrite in vitro and its rapid removal from DNA by depurination. *FEBS Lett.*, **376**, 207–210.
8. Tuo,J., Liu,L., Poulsen,H.E., Weimann,A., Svendsen,O. and Loft,S. (2000) Importance of guanine nitration and hydroxylation in DNA in vitro and in vivo. *Free Radic Biol Med*, **29**, 147–155.
9. Friedberg,E.C., Walker,G.C., Siede,W., Wood,R.D. and Ellenberger,T. (2005) In: *DNA Repair and Mutagenesis*. ASM Press.
10. Friedberg,E.C. (2005) Suffering in silence: the tolerance of DNA damage. *Nat. Rev. Mol. Cell Biol.*, **6**, 943–953.
11. Lawrence,C.W. and Christensen,R.B. (1978) Ultraviolet-induced reversion of *cyc1* alleles in radiation-sensitive strains of yeast. I. *rev1* mutant strains. *J. Mol. Biol.*, **122**, 1–21.
12. Lawrence,C.W. and Christensen,R.B. (1979) Ultraviolet-induced reversion of *cyc1* alleles in radiation-sensitive strains of yeast. III. *rev3* mutant strains. *Genetics*, **92**, 397–408.
13. Yu,S.L., Johnson,R.E., Prakash,S. and Prakash,L. (2001) Requirement of DNA polymerase eta for error-free bypass of UV-induced CC and TC photoproducts. *Mol. Cell. Biol.*, **21**, 185–188.
14. Kozmin,S.G., Pavlov,Y.I., Kunkel,T.A. and Sage,E. (2003) Roles of *Saccharomyces cerevisiae* DNA polymerases poleta and polzeta in response to irradiation by simulated sunlight. *Nucleic Acids Res.*, **31**, 4541–4552.
15. Sakamoto,A.N. (2019) Translesion synthesis in plants: ultraviolet resistance and beyond. *Front. Plant Sci.*, **10**, 1208.
16. Nakagawa,M., Takahashi,S., Tanaka,A., Narumi,I. and Sakamoto,A.N. (2011) Role of Atpolzeta, Atrev1, and Atpoleta in UV light-induced mutagenesis in Arabidopsis. *Plant Physiol.*, **155**, 414–420.
17. Yousefzadeh,M.J. and Wood,R.D. (2013) DNA polymerase POLQ and cellular defense against DNA damage. *DNA Repair (Amst.)*, **12**, 1–9.
18. Seki,M., Masutani,C., Yang,L.W., Schuffert,A., Iwai,S., Bahar,I. and Wood,R.D. (2004) High-efficiency bypass of DNA damage by human DNA polymerase Q. *EMBO J.*, **23**, 4484–4494.
19. Hogg,M., Seki,M., Wood,R.D., Doublie,S. and Wallace,S.S. (2011) Lesion bypass activity of DNA polymerase theta (POLQ) is an intrinsic property of the pol domain and depends on unique sequence inserts. *J. Mol. Biol.*, **405**, 642–652.
20. Hogg,M., Sauer-Eriksson,A.E. and Johansson,E. (2012) Promiscuous DNA synthesis by human DNA polymerase theta. *Nucleic Acids Res.*, **40**, 2611–2622.
21. Laverty,D.J., Averill,A.M., Doublie,S. and Greenberg,M.M. (2017) The A-rule and deletion formation during abasic and oxidized abasic site bypass by DNA polymerase theta. *ACS Chem. Biol.*, **12**, 1584–1592.
22. Laverty,D.J. and Greenberg,M.M. (2017) In vitro bypass of thymidine glycol by DNA polymerase theta forms sequence-dependent frameshift mutations. *Biochemistry*, **56**, 6726–6733.
23. Sale,J.E. (2013) Translesion DNA synthesis and mutagenesis in eukaryotes. *Cold Spring Harb. Perspect. Biol.*, **5**, a012708.
24. Conde,J., Yoon,J.H., Roy,C.J., Prakash,L. and Prakash,S. (2015) Genetic control of replication through N1-methyladenine in human cells. *J. Biol. Chem.*, **290**, 29794–29800.
25. Yoon,J.H., Hodge,R.P., Hackfeld,L.C., Park,J., Roy,C.J., Prakash,S. and Prakash,L. (2018) Genetic control of predominantly error-free replication through an acrolein-derived minor-groove DNA adduct. *J. Biol. Chem.*, **293**, 2949–2958.
26. Yoon,J.H., Johnson,R.E., Prakash,L. and Prakash,S. (2019) DNA polymerase theta accomplishes translesion synthesis opposite 1,N(6)-ethenodeoxyadenosine with a remarkably high fidelity in human cells. *Genes Dev.*, **33**, 282–287.
27. Yoon,J.H., Roy,C.J., Park,J., Prakash,S. and Prakash,L. (2014) A role for DNA polymerase theta in promoting replication through oxidative DNA lesion, thymine glycol, in human cells. *J. Biol. Chem.*, **289**, 13177–13185.
28. Yoon,J.H., McArthur,M.J., Park,J., Basu,D., Wakamiya,M., Prakash,L. and Prakash,S. (2019) Error-prone replication through UV lesions by DNA polymerase theta protects against skin cancers. *Cell*, **176**, 1295–1309.
29. Kohzaki,M., Nishihara,K., Hirota,K., Sonoda,E., Yoshimura,M., Ekino,S., Butler,J.E., Watanabe,M., Halazonetis,T.D. and Takeda,S. (2010) DNA polymerases nu and theta are required for efficient

immunoglobulin v gene diversification in chicken. *J. Cell Biol.*, **189**, 1117–1127.
30. Zahn,K.E., Jensen,R.B., Wood,R.D. and Doublie,S. (2021) Human DNA polymerase theta harbors DNA end-trimming activity critical for DNA repair. *Mol. Cell*, **81**, 1534–1547.
31. Plecenikova,A., Slaninova,M. and Riha,K. (2014) Characterization of DNA repair deficient strains of *Chlamydomonas reinhardtii* generated by insertional mutagenesis. *PLoS One*, **9**, e105482.
32. Kamisugi,Y., Whitaker,J.W. and Cuming,A.C. (2016) The transcriptional response to DNA-Double-Strand breaks in *Physcomitrella patens*. *PLoS One*, **11**, e0161204.
33. Inagaki,S., Suzuki,T., Ohto,M.A., Urawa,H., Horiuchi,T., Nakamura,K. and Morikami,A. (2006) Arabidopsis TEBICHI, with helicase and DNA polymerase domains, is required for regulated cell division and differentiation in meristems. *Plant Cell*, **18**, 879–892.
34. Inagaki,S., Nakamura,K. and Morikami,A. (2009) A link among DNA replication, recombination, and gene expression revealed by genetic and genomic analysis of *TEBICHI* gene of *Arabidopsis thaliana*. *PLoS Genet.*, **5**, e1000613.
35. van Kregten,M., de Pater,S., Romeijn,R., van Schendel,R., Hooykaas,P.J. and Tijsterman,M. (2016) T-DNA integration in plants results from polymerase-theta-mediated DNA repair. *Nat Plants*, **2**, 16164.
36. Nishizawa-Yokoi,A., Saika,H., Hara,N., Lee,L.Y., Toki,S. and Gelvin,S.B. (2021) *Agrobacterium* T-DNA integration in somatic cells does not require the activity of DNA polymerase θ. *New Phytol.*, **229**, 2859–2872.
37. Mara,K., Charlot,F., Guyon-Debast,A., Schaefer,D.G., Collonnier,C., Grelon,M. and Nogué,F. (2019) POLQ plays a key role in the repair of CRISPR/Cas9-induced double-stranded breaks in the moss *Physcomitrella patens*. *New Phytol.*, **222**, 1380–1391.
38. Xia,J., Kong,D., Xue,S., Tian,W., Li,N., Bao,F., Hu,Y., Du,J., Wang,Y., Pan,X. *et al.* (2014) Nitric oxide negatively regulates AKT1-mediated potassium uptake through modulating vitamin B6 homeostasis in Arabidopsis. *Proc. Natl. Acad. Sci. U.S.A.*, **111**, 16196–16201.
39. Lv,Q., Wang,L., Wang,J.Z., Li,P., Chen,Y.L., Du,J., He,Y.K. and Bao,F. (2017) SHB1/HY1 alleviates excess boron stress by increasing BOR4 expression level and maintaining boron homeostasis in Arabidopsis roots. *Front. Plant Sci.*, **8**, 790.
40. Wang,S., Wen,R., Shi,X., Lambrecht,A., Wang,H. and Xiao,W. (2011) RAD5a and REV3 function in two alternative pathways of DNA-damage tolerance in Arabidopsis. *DNA Repair (Amst.)*, **10**, 620–628.
41. Wolter,F., Schindele,P., Beying,N., Scheben,A. and Puchta,H. (2021) Different DNA repair pathways are involved in single-strand break-induced genomic changes in plants. *Plant Cell*, **33**, 3454–3469.
42. Streatfield,S.J., Weber,A., Kinsman,E.A., Hausler,R.E., Li,J., Post-Beittenmiller,D., Kaiser,W.M., Pyke,K.A., Flugge,U.I. and Chory,J. (1999) The phosphoenolpyruvate/phosphate translocator is required for phenolic metabolism, palisade cell development, and plastid-dependent nuclear gene expression. *Plant Cell*, **11**, 1609–1622.
43. Feechan,A., Kwon,E., Yun,B.W., Wang,Y., Pallas,J.A. and Loake,G.J. (2005) A central role for S-nitrosothiols in plant disease resistance. *Proc. Natl. Acad. Sci. U.S.A.*, **102**, 8054–8059.
44. Han,B., Yang,Z., Xie,Y., Nie,L., Cui,J. and Shen,W. (2014) Arabidopsis HY1 confers cadmium tolerance by decreasing nitric oxide production and improving iron homeostasis. *Mol Plant*, **7**, 388–403.
45. Corpas,F.J., Hayashi,M., Mano,S., Nishimura,M. and Barroso,J.B. (2009) Peroxisomes are required for in vivo nitric oxide accumulation in the cytosol following salinity stress of Arabidopsis plants. *Plant Physiol.*, **151**, 2083–2094.
46. Pacurar,D.I., Pacurar,M.L., Street,N., Bussell,J.D., Pop,T.I., Gutierrez,L. and Bellini,C. (2012) A collection of INDEL markers for map-based cloning in seven Arabidopsis accessions. *J. Exp. Bot.*, **63**, 2491–2501.
47. Yoo,S.D., Cho,Y.H. and Sheen,J. (2007) Arabidopsis mesophyll protoplasts: a versatile cell system for transient gene expression analysis. *Nat. Protoc.*, **2**, 1565–1572.
48. Schmittgen,T.D. and Livak,K.J. (2008) Analyzing real-time PCR data by the comparative C(T) method. *Nat. Protoc.*, **3**, 1101–1108.
49. Epe,B., Ballmaier,D., Roussyn,I., Briviba,K. and Sies,H. (1996) DNA damage by peroxynitrite characterized with DNA repair enzymes. *Nucleic Acids Res.*, **24**, 4105–4110.
50. Sakamoto,T., Inui,Y.T., Uraguchi,S., Yoshizumi,T., Matsunaga,S., Mastui,M., Umeda,M., Fukui,K. and Fujiwara,T. (2011) Condensin II alleviates DNA damage and is essential for tolerance of boron overload stress in Arabidopsis. *Plant Cell*, **23**, 3533–3546.
51. Friesner,J.D., Liu,B., Culligan,K. and Britt,A.B. (2005) Ionizing radiation-dependent gamma-H2AX focus formation requires ataxia telangiectasia mutated and ataxia telangiectasia mutated and Rad3-related. *Mol. Biol. Cell*, **16**, 2566–2576.
52. Amiard,S., Charbonnel,C., Allain,E., Depeiges,A., White,C.I. and Gallego,M.E. (2010) Distinct roles of the ATR kinase and the Mre11-Rad50-Nbs1 complex in the maintenance of chromosomal stability in Arabidopsis. *Plant Cell*, **22**, 3020–3033.
53. Menke,M., Chen,I., Angelis,K.J. and Schubert,I. (2001) DNA damage and repair in *Arabidopsis thaliana* as measured by the comet assay after treatment with different classes of genotoxins. *Mutat. Res.*, **493**, 87–93.
54. Doyle,J. and Doyle,J.L. (1990) Isolation of plant DNA from fresh tissue. *Focus (San Francisco, Calif.)*, **12**, 13–15.
55. G.,C. (2016) 1,135 Genomes reveal the global pattern of polymorphism in *Arabidopsis thaliana*. *Cell*, **166**, 481–491.
56. Bethke,P.C., Libourel,I.G., Reinöhl,V. and Jones,R.L. (2006) Sodium nitroprusside, cyanide, nitrite, and nitrate break Arabidopsis seed dormancy in a nitric oxide-dependent manner. *Planta*, **223**, 805–812.
57. Guo,F.Q., Okamoto,M. and Crawford,N.M. (2003) Identification of a plant nitric oxide synthase gene involved in hormonal signaling. *Science*, **302**, 100–103.
58. Zhou,J., Gelot,C., Pantelidou,C., Li,A., Yucel,H., Davis,R.E., Farkkila,A., Kochupurakkal,B., Syed,A., Shapiro,G.I. *et al.* (2021) A first-in-class polymerase theta inhibitor selectively targets homologous-recombination-deficient tumors. *Nat. Cancer*, **2**, 598–610.
59. Ceccaldi,R., Liu,J.C., Amunugama,R., Hajdu,I., Primack,B., Petalcorin,M.I., O'Connor,K.W., Konstantinopoulos,P.A., Elledge,S.J., Boulton,S.J. *et al.* (2015) Homologous-recombination-deficient tumours are dependent on Poltheta-mediated repair. *Nature*, **518**, 258–262.
60. Mateos-Gomez,P.A., Gong,F., Nair,N., Miller,K.M., Lazzerini-Denchi,E. and Sfeir,A. (2015) Mammalian polymerase theta promotes alternative NHEJ and suppresses recombination. *Nature*, **518**, 254–257.
61. Schimmel,J., van Schendel,R., den Dunnen,J.T. and Tijsterman,M. (2019) Templated insertions: a smoking gun for polymerase theta-mediated end joining. *Trends Genet.*, **35**, 632–644.
62. Ramsden,D.A., Carvajal-Garcia,J. and Gupta,G.P. (2022) Mechanism, cellular functions and cancer roles of polymerase-theta-mediated DNA end joining. *Nat. Rev. Mol. Cell Biol.*, **23**, 125–140.
63. Huang,C.H., Mirabelli,C.K., Jan,Y. and Crooke,S.T. (1981) Single-strand and double-strand deoxyribonucleic acid breaks produced by several bleomycin analogues. *Biochemistry*, **20**, 233–238.
64. Liu,C.H., Finke,A., Diaz,M., Rozhon,W., Poppenberger,B., Baubec,T. and Pecinka,A. (2015) Repair of DNA damage induced by the cytidine analog zebularine requires ATR and ATM in Arabidopsis. *Plant Cell*, **27**, 1788–1800.
65. Gentric,N., Masoud,K., Journot,R.P., Cognat,V., Chaboute,M.E., Noir,S. and Genschik,P. (2020) The F-Box-Like protein FBL17 is a regulator of DNA-damage response and colocalizes with RETINOBLASTOMA RELATED1 at DNA lesion sites. *Plant Physiol.*, **183**, 1295–1305.
66. Carvajal-Garcia,J., Cho,J.E., Carvajal-Garcia,P., Feng,W., Wood,R.D., Sekelsky,J., Gupta,G.P., Roberts,S.A. and Ramsden,D.A. (2020) Mechanistic basis for microhomology identification and genome scarring by polymerase theta. *Proc. Natl. Acad. Sci. U.S.A.*, **117**, 8476–8485.
67. Moore,G., Majumdar,R., Powell,S.N., Khan,A.J., Weinhold,N., Yin,S. and Higginson,D.S. (2022) Templated insertions are associated specifically with BRCA2 deficiency and overall survival in advanced ovarian cancer. *Mol. Cancer Res.*, **21**, 1012.
68. Ceccaldi,R., Rondinelli,B. and D'Andrea,A.D. (2016) Repair pathway choices and consequences at the double-strand break. *Trends Cell Biol.*, **26**, 52–64.

69. Huie,R.E. and Padmaja,S. (1993) The reaction of no with superoxide. *Free Radic. Res. Commun.*, **18**, 195–199.
70. Delledonne,M., Zeier,J., Marocco,A. and Lamb,C. (2001) Signal interactions between nitric oxide and reactive oxygen intermediates in the plant hypersensitive disease resistance response. *Proc. Natl. Acad. Sci. U.S.A.*, **98**, 13454–13459.
71. Menges,M., de Jager,S.M., Gruissem,W. and Murray,J.A. (2005) Global analysis of the core cell cycle regulators of Arabidopsis identifies novel genes, reveals multiple and highly specific profiles of expression and provides a coherent model for plant cell cycle control. *Plant J.*, **41**, 546–566.
72. Yoshizumi,T., Tsumoto,Y., Takiguchi,T., Nagata,N., Yamamoto,Y.Y., Kawashima,M., Ichikawa,T., Nakazawa,M., Yamamoto,N. and Matsui,M. (2006) Increased level of polyploidy1, a conserved repressor of CYCLINA2 transcription, controls endoreduplication in Arabidopsis. *Plant Cell*, **18**, 2452–2468.
73. Yoon,J.H., Roy,C.J., Park,J., Prakash,S. and Prakash,L. (2017) Translesion synthesis DNA polymerases promote error-free replication through the minor-groove DNA adduct 3-deaza-3-methyladenine. *J. Biol. Chem.*, **292**, 18682–18688.
74. Daigaku,Y., Davies,A.A. and Ulrich,H.D. (2010) Ubiquitin-dependent DNA damage bypass is separable from genome replication. *Nature*, **465**, 951–955.
75. Karras,G.I. and Jentsch,S. (2010) The RAD6 DNA damage tolerance pathway operates uncoupled from the replication fork and is functional beyond s phase. *Cell*, **141**, 255–267.
76. Fan,L., Bi,T., Wang,L. and Xiao,W. (2020) DNA-damage tolerance through PCNA ubiquitination and sumoylation. *Biochem. J.*, **477**, 2655–2677.
77. Burney,S., Caulfield,J.L., Niles,J.C., Wishnok,J.S. and Tannenbaum,S.R. (1999) The chemistry of DNA damage from nitric oxide and peroxynitrite. *Mutat. Res.*, **424**, 37–49.
78. Khan,F.H., Dervan,E., Bhattacharyya,D.D., McAuliffe,J.D., Miranda,K.M. and Glynn,S.A. (2020) The role of nitric oxide in cancer: master regulator or NOt? *Int. J. Mol. Sci.*, **21**, 9393.
79. Lee,D.H. and Pfeifer,G.P. (2007) Mutagenesis induced by the nitric oxide donor sodium nitroprusside in mouse cells. *Mutagenesis*, **22**, 63–67.
80. Bai,S., Li,M., Yao,T., Wang,H., Zhang,Y., Xiao,L., Wang,J., Zhang,Z., Hu,Y., Liu,W. *et al.* (2012) Nitric oxide restrain root growth by DNA damage induced cell cycle arrest in *Arabidopsis thaliana*. *Nitric Oxide*, **26**, 54–60.
81. Fulcher,N. and Sablowski,R. (2009) Hypersensitivity to DNA damage in plant stem cell niches. *Proc. Natl. Acad. Sci. U.S.A.*, **106**, 20984–20988.
82. Schrempf,A., Slyskova,J. and Loizou,J.I. (2021) Targeting the DNA repair enzyme polymerase theta in cancer therapy. *Trends Cancer*, **7**, 98–111.
83. Wu,X., Takenaka,K., Sonoda,E., Hochegger,H., Kawanishi,S., Kawamoto,T., Takeda,S. and Yamazoe,M. (2006) Critical roles for polymerase zeta in cellular tolerance to nitric oxide-induced DNA damage. *Cancer Res.*, **66**, 748–754.
84. Nisa,M., Bergis,C., Pedroza-Garcia,J.A., Drouin-Wahbi,J., Mazubert,C., Bergounioux,C., Benhamed,M. and Raynaud,C. (2021) The plant DNA polymerase theta is essential for the repair of replication-associated DNA damage. *Plant J.*, **106**, 1197–1207.
85. Prasad,R., Longley,M.J., Sharief,F.S., Hou,E.W., Copeland,W.C. and Wilson,S.H. (2009) Human DNA polymerase theta possesses 5'-dRP lyase activity and functions in single-nucleotide base excision repair in vitro. *Nucleic Acids Res.*, **37**, 1868–1877.
86. Yoshimura,M., Kohzaki,M., Nakamura,J., Asagoshi,K., Sonoda,E., Hou,E., Prasad,R., Wilson,S.H., Tano,K., Yasui,A. *et al.* (2006) Vertebrate POLQ and POLbeta cooperate in base excision repair of oxidative DNA damage. *Mol. Cell*, **24**, 115–125.
87. Roldan-Arjona,T., Ariza,R.R. and Cordoba-Canero,D. (2019) DNA base excision repair in plants: an unfolding story with familiar and novel characters. *Front. Plant Sci.*, **10**, 1055.
88. Ohshima,H., Sawa,T. and Akaike,T. (2006) 8-nitroguanine, a product of nitrative DNA damage caused by reactive nitrogen species: formation, occurrence, and implications in inflammation and carcinogenesis. *Antioxid. Redox. Signal.*, **8**, 1033–1045.
89. Tretyakova,N.Y., Burney,S., Pamir,B., Wishnok,J.S., Dedon,P.C., Wogan,G.N. and Tannenbaum,S.R. (2000) Peroxynitrite-induced DNA damage in the *supF* gene: correlation with the mutational spectrum. *Mutat. Res.*, **447**, 287–303.
90. Tretyakova,N.Y., Wishnok,J.S. and Tannenbaum,S.R. (2000) Peroxynitrite-induced secondary oxidative lesions at guanine nucleobases: chemical stability and recognition by the Fpg DNA repair enzyme. *Chem. Res. Toxicol.*, **13**, 658–664.
91. Cordoba-Canero,D., Roldan-Arjona,T. and Ariza,R.R. (2014) Arabidopsis ZDP DNA 3'-phosphatase and ARP endonuclease function in 8-oxoG repair initiated by FPG and OGG1 DNA glycosylases. *Plant J.*, **79**, 824–834.
92. Routledge,M.N. (2000) Mutations induced by reactive nitrogen oxide species in the *supF* forward mutation assay. *Mutat. Res.*, **450**, 95–105.
93. Jiang,C., Mithani,A., Belfield,E.J., Mott,R., Hurst,L.D. and Harberd,N.P. (2014) Environmentally responsive genome-wide accumulation of de novo *Arabidopsis thaliana* mutations and epimutations. *Genome Res.*, **24**, 1821–1829.
94. Goyal,V., Jhanghel,D. and Mehrotra,S. (2021) Emerging warriors against salinity in plants: nitric oxide and hydrogen sulphide. *Physiol. Plant.*, **171**, 896–908.
95. Iqbal,N., Umar,S., Khan,N.A. and Corpas,F.J. (2021) Crosstalk between abscisic acid and nitric oxide under heat stress: exploring new vantage points. *Plant Cell Rep.*, **40**, 1429–1450.
96. Chen,T., Chen,X., Zhang,S., Zhu,J., Tang,B., Wang,A., Dong,L., Zhang,Z., Yu,C., Sun,Y. *et al.* (2021) The genome sequence archive family: toward explosive data growth and diverse data types. *Genomics Proteomics Bioinformatics*, **19**, 578–583.
97. CNCB-NGDC Members and Partners (2021) Database resources of the national genomics data center, china national center for bioinformation in 2021. *Nucleic Acids Res.*, **49**, D18–D28.